

JGR Solid Earth



RESEARCH ARTICLE

10.1029/2020JB021243

Key Points:

- Hypotheses for southern African Plateau uplift are tested using large-scale landscape model inversions
- Comparison of models to published thermochronology, sediment flux volumes, and topography highlight four suitable uplift histories
- Best fit models either show Cretaceous uplift only or a hybrid of Cretaceous and Cenozoic uplift with different geodynamic implications

Supporting Information:

Supporting Information may be found in the online version of this article.

Correspondence to:

J. R. Stanley,
jessicastanley@uidaho.edu







Citation:

Stanley, J. R., Braun, J., Baby, G., Guillocheau, F., Robin, C., Flowers, R. M., et al. (2021). Constraining plateau uplift in southern Africa by combining thermochronology, sediment flux, topography, and landscape evolution modeling. *Journal of Geophysical Research: Solid Earth*, 126, e2020JB021243. <https://doi.org/10.1029/2020JB021243>

Received 29 OCT 2020

Accepted 24 JUN 2021

Constraining Plateau Uplift in Southern Africa by Combining Thermochronology, Sediment Flux, Topography, and Landscape Evolution Modeling

Jessica R. Stanley^{1,2} , Jean Braun^{2,3} , Guillaume Baby⁴ , François Guillocheau⁵, Cécile Robin⁵, Rebecca M. Flowers⁶ , Roderick Brown⁷, Mark Wildman⁷ , and Romain Beucher⁸ 

¹Department of Geological Sciences, University of Idaho, Moscow, USA, ²Helmholtz Centre Potsdam, GFZ German Research Center for Geosciences, Potsdam, Germany, ³Institut für Erd- und Umweltwissenschaften, Universität Potsdam, Potsdam, Germany, ⁴Université de Paris, Institut de Physique du Globe de Paris, CNRS, Paris, France, ⁵Université de Rennes 1, CNRS, Géosciences Rennes - UMR 6118, Rennes, France, ⁶Department of Geological Sciences, University of Colorado Boulder, Boulder, CO, USA, ⁷School of Geographical and Earth Sciences, University of Glasgow, Glasgow, Scotland, ⁸Research School of Earth Sciences, The Australian National University, Canberra, ACT, Australia

Abstract The uplift of the southern African Plateau with its average elevations of ~1,000 m is often attributed to mantle processes, but there are conflicting theories for the timing and drivers of topographic development. Evidence for most proposed plateau development histories is derived from continental erosion histories, marine stratigraphic architecture, or landscape morphology. Here we use a landscape evolution model to integrate a large data set of low-temperature thermochronometry, sediment flux rates to surrounding marine basins, and current topography for southern Africa. We explore three main hypotheses for surface uplift: (a) southern Africa was already elevated by the Early Cretaceous before Gondwana breakup, (b) uplift and continental tilting occurred during the mid-Cretaceous, or (c) uplift occurred during the mid to late Cenozoic. We test which of these three intervals of plateau development are plausible by using an inversion method to constrain the range in erosional and uplift model parameters that can best reproduce the observed data. Results indicate four regions of parameter space that fall into two families of uplift histories are most compatible with the data. Both uplift families have limited initial topography with some topographic uplift and continental tilting starting at ~90–100 Ma. In one acceptable scenario, nearly all of the topography, >1,300 m, is created at this time with little Cenozoic uplift. In the other acceptable scenario, ~400–800 m of uplift occurs in the mid-Cretaceous with another ~500–1,000 m of uplift in the mid-Cenozoic. The two model scenarios have different geodynamic implications, which we compare to geodynamic models.

Plain Language Summary How the southern African Plateau and its high elevations formed is disputed. The plateau is located far from tectonic plate boundaries, and many have suggested that processes below the crust are responsible for plateau uplift. Here, we use a wide range of data that documents the long-term erosion history of the plateau and a landscape evolution model to test proposed uplift histories. Model results show two types of plateau uplift histories that can adequately match the data. One suggests that all the plateau was uplifted rapidly ~90–100 million years ago. The other suggests two phases of uplift, one ~90–100 million years ago, and a second <40 million years ago. We cannot indicate which one is correct with the data that we included, but the results have different implications for processes occurring in the deep earth.

1. Introduction

The southern African Plateau is a dominant feature of African topography reaching heights of >3,000 m, with an average elevation of 1,000 m in the predominantly low relief plateau interior. The elevated margins of the plateau drop through higher relief regions to the coastal plain (Figure 1). However, extensive debate remains regarding when and how it formed. The long wavelength topographic high in absence of collisional tectonism combined with Cretaceous kimberlite activity and a large low shear velocity province (LLSVP) in the deep mantle below southern Africa have led many to suggest uplift related to mantle processes. Given that surface uplift may be related to LLSVP development (e.g., Lithgow-Bertelloni & Silver, 1998), better

© 2021. The Authors.

This is an open access article under the terms of the [Creative Commons Attribution-NonCommercial License](https://creativecommons.org/licenses/by-nc/4.0/), which permits use, distribution and reproduction in any medium, provided the original work is properly cited and is not used for commercial purposes.

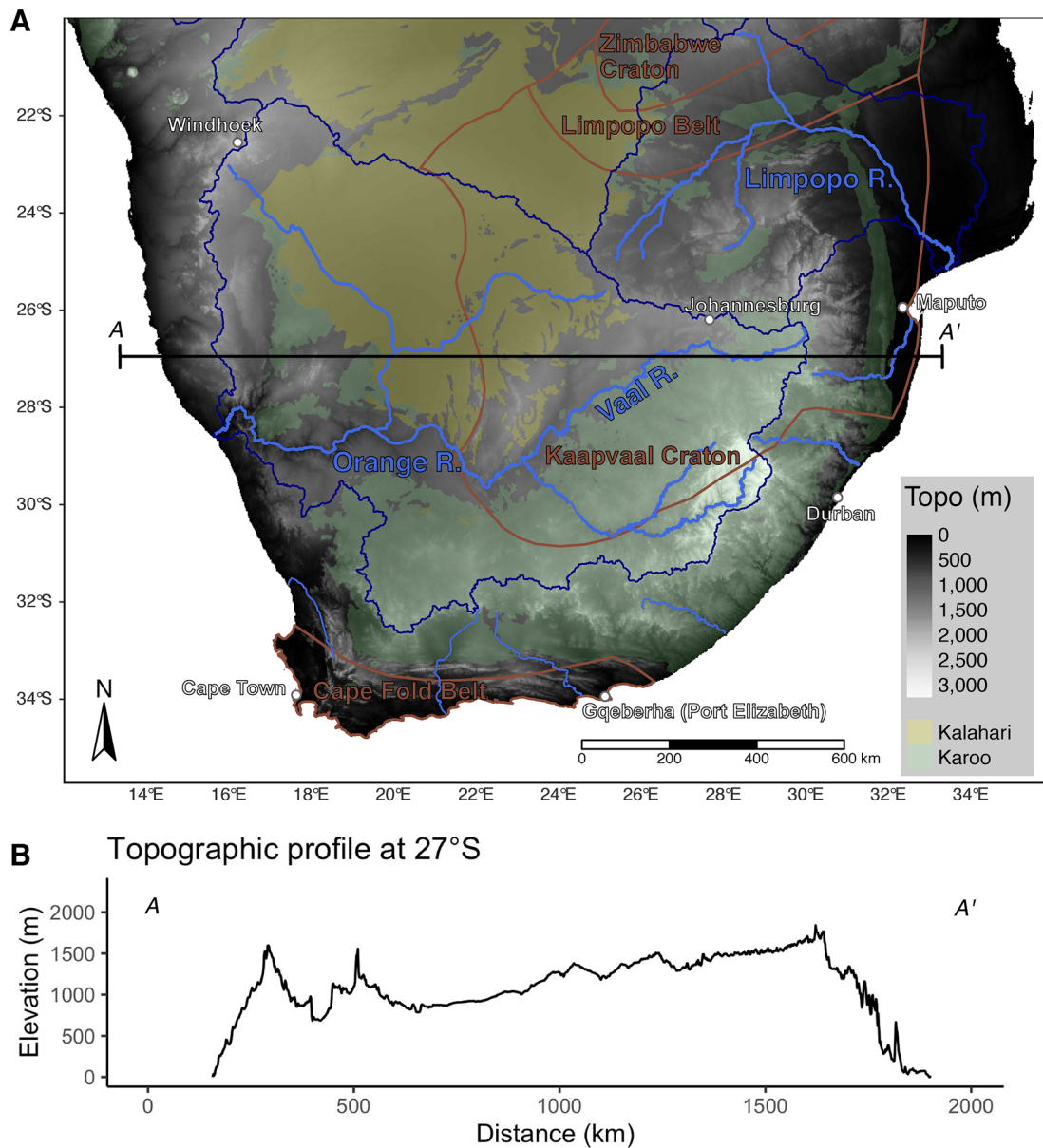


Figure 1. Topography and simplified geology. (a) Topography and simplified basement and post 300-Ma geology for southern Africa. Dark blue lines show main drainage divides and bright blue lines and labels show main rivers including the Orange-Vaal and Limpopo river systems. Green shading denotes the extent of the Permian to Jurassic Karoo sedimentary basin, Jurassic Karoo volcanic rocks and sills, and early Cretaceous Etendeka volcanic rocks. Yellow shading shows the extent of the thin, Cenozoic Kalahari Basin deposits. Brown outlines show major basement domains mentioned in text. (b) Topographic profile across 27°S, section line A–A' shown on map.

constraints on the timing of uplift could provide additional information on the nature and development of this deep seismic anomaly and other mantle processes that may cause southern Africa's anomalous elevations (e.g., Gurnis et al., 2000).

Overall, three main intervals have been proposed for when most of the uplift occurred in southern Africa (summarized in Table 1). First, the plateau may already have been elevated before 130 Ma due to processes that occurred prior to or associated with Gondwana breakup. Hypothesized geodynamic mechanisms to achieve uplift at this time include thermal uplift and crustal thickening due to large igneous provinces (LIPs, e.g., Cox, 1989), isostatic rebound after dynamic subsidence and deposition of the continental Karoo Basin (Pysklywec & Mitrovica, 1999), and inherited topography (Doucouré & de Wit, 2003). Most of the

Table 1
Proposed Geodynamic Mechanisms and Evidence for Proposed Stages of Uplift

Timing	Geodynamic mechanism	Evidence
Before or during Gondwana breakup (>130 Ma)	<ul style="list-style-type: none"> Thermal uplift and crustal thickening associated with LIP activity¹ Isostatic rebound after dynamic subsidence and deposition of the Karoo basin² Inherited Paleozoic topography³ Flexural uplift from far field plate stresses^{4,5} 	<ul style="list-style-type: none"> Major phase of cooling in AFT thermochronology studies around the margins just after rifting^{6,7,8,9,10,11} Models of escarpment retreat developed in S. Africa suggest some topography at breakup^{12,13} and a pre-existing topographic divide¹⁴ Radial drainages around LIPs¹
Mid-Cretaceous (110–80 Ma)	<ul style="list-style-type: none"> Dynamic topography due to the LLSVP in the deep mantle^{15,16} Changes to the lithospheric density structure^{17,18}, long lived plume tails¹⁹, and/or delamination²⁰ associated with kimberlite magmatism Pressure driven flow in the asthenosphere²¹ Flexural uplift from far field plate stresses^{4,5} Agulhas LIP off the S coast at ~90 Ma²² 	<ul style="list-style-type: none"> Phase of cooling seen in AFT^{7,8,9,10,23,24} (Brown et al., 2002; Gallagher & Brown, 1999a, 1999b; Kounov et al., 2009; Tinker et al., 2008b; Wildman et al., 2015) and AHe^{17,25,26,27,28,29} Major pulse of sediment delivered to the marine basins off the western and southern coasts^{30,31,32,33} Geometric evidence from offshore forced regressive wedges, margin tilting, and incised valleys³⁰
Mid- to Late Cenozoic (<35 Ma)	<ul style="list-style-type: none"> Small-scale convection in the upper mantle due to the slowing of African plate at ~30 Ma^{34,35,36} Dynamic topography due to density variations in the upper mantle and/or the LLSVP^{15,37,38,39,40,41} Flexural uplift from far field plate stresses^{4,5} 	<ul style="list-style-type: none"> Large-scale correlation of geomorphic surfaces^{35,42,43} River profiles and models of their formation through time^{40,44,45} Terraces on the lower Orange River⁴⁶ Geometric evidence from offshore forced regressive wedges and margin tilting³⁰ Inferred cooling phase on the southern coast from modeling of AFT data⁴⁷

Note. ¹Cox (1989), ²Pysklywec and Mitrovica (1999), ³Doucouré and de Wit (2003), ⁴Moore (1999), ⁵Moore et al. (2009), ⁶Brown et al. (1990), ⁷Brown et al. (2002), ⁸Gallagher and Brown (1999a), ⁹Tinker et al. (2008b), ¹⁰Wildman et al. (2015), ¹¹Wildman et al. (2016), ¹²Gilchrist et al. (1994), ¹³Gilchrist and Summerfield (1990), Van Der Beek et al. (2002), ¹⁴Braun et al. (2014), ¹⁵Lithgow-Bertelloni and Silver (1998), ¹⁶Bell et al. (2003), ¹⁷Stanley et al. (2013), ¹⁸Nyblade and Sleep (2003), ¹⁹Hu et al. (2018), ²¹Colli et al. (2014), ²²M. de Wit (2007), ²³Gallagher and Brown (1999b), ²⁴Kounov et al. (2009), ²⁵Flowers and Schoene (2010), ²⁶Kounov et al. (2013), ²⁷Stanley et al. (2015), ²⁸Stanley and Flowers (2020), ²⁹Wildman et al. (2017), ³⁰Baby et al. (2020), ³¹Guillocheau et al. (2012), ³²Rouby et al. (2009), ³³Tinker et al. (2008a), ³⁴Burke (1996), ³⁵Burke and Gunnell (2008), ³⁶Burke and Wilson (1972), ³⁷Al-Hajri et al. (2009), ³⁸Gurnis et al. (2000), ³⁹Moucha and Forte (2011), ⁴⁰Paul et al. (2014), ⁴¹Winterbourne et al. (2009), ⁴²King (1942), ⁴³Partridge and Maud (1987), ⁴⁴Roberts and White (2010), ⁴⁵Rudge et al. (2015), ⁴⁶Dauteuil et al. (2015), ⁴⁷Green et al. (2017).

supporting evidence for pre-130 Ma uplift is based on the morphology of rift flank uplifts, their erosion, and models for their evolution (e.g., Gilchrist et al., 1994; Gilchrist & Summerfield, 1990; Van Der Beek et al., 2002). Alternatively, uplift may have occurred 100–80 Ma. This timing is supported by a major pulse of continental erosion detected by thermochronology and marine sediment flux (e.g., Baby et al., 2020; Flowers & Schoene, 2010; Gallagher & Brown, 1999b; Guillocheau et al., 2012; Kounov et al., 2013; Stanley et al., 2013; Tinker et al., 2008a; Wildman et al., 2015). Many geodynamic mechanisms have been proposed to generate plateau uplift at this time (see Table 1), but the two most commonly invoked are dynamic topography due to the LLSVP (e.g., Braun et al., 2014; Lithgow-Bertelloni & Silver, 1998) or changes in lithospheric buoyancy associated with kimberlite magmatism (e.g., Hu et al., 2018; Stanley et al., 2013; Tinker et al., 2008b). Continent-wide tilting has been shown to be important during this phase (Braun et al., 2014), and potentially caused by either motion of the African plate onto a dynamic topography high above the LLSVP (Braun et al., 2014), or delamination and/or changes in lithospheric buoyancy with the east to west progression of kimberlites (Bell et al., 2003; Hu et al., 2018). Finally, uplift may have occurred after ~30 Ma. This is usually attributed to dynamic topography and small-scale convection in the upper mantle (e.g., Al-Hajri et al., 2009; Burke, 1996), though others suggest that the LLSVP developed during this period (Al-Hajri et al., 2009; Gurnis et al., 2000). Evidence for Cenozoic uplift is dominantly based on mapping of planation surfaces (e.g., Burke, 1996; Burke & Gunnell, 2008; King, 1942, 1950; Partridge & Maud, 1987), river profile analysis (e.g., Paul et al., 2014; Roberts & White, 2010; Rudge et al., 2015), or stratigraphic data (tilting and truncation of the margin, forced regressive wedges, e.g., Baby, Guillocheau, Morin, et al., 2018).

Some authors (Baby et al., 2020) suggest a two steps-uplift of the southern Africa Plateau, at 93–70 (tilting of the plateau) and 25–15 Ma (Indian Ocean side only).

The timing and patterns of uplift are key for resolving the driving mechanisms, but because topographic uplift is difficult to discern directly from the continental rock record there remains discussion on how extensive surface uplift was during each of these three intervals. Direct proxies for paleoelevation are rare and commonly surface uplift is inferred based on the assertion that topographic uplift generates relief which triggers an erosional response that is easier to detect in the rock record. Extensive work using thermochronology and quantifying sediment flux to the marine basins gives a fairly complete picture of the long-term erosion and sedimentation history in southern Africa (Baby, Guillocheau, Boulogne, et al., 2018; Baby et al., 2020; Baby, Guillocheau, Morin, et al., 2018; Belton & Raab, 2010; Brown et al., 1990, 2002, 2014; Flowers & Schoene, 2010; Gallagher & Brown, 1999a, 1999b; Green et al., 2017; Guillocheau et al., 2012; Kounov et al., 2009, 2013; Raab et al., 2002; Rouby et al., 2009; Said et al., 2015; Stanley & Flowers, 2020; Stanley et al., 2013, 2015; Tinker et al., 2008a, 2008b; Wildman et al., 2015, 2016, 2017), but the magnitude of surface uplift required to drive the erosion is not known. Additionally, the morphology of the landscape should contain signatures of the uplift history (e.g., Burke, 1996; Burke & Gunnell, 2008; Partridge & Maud, 1987; Roberts & White, 2010) but the timing and rate of formation of these geomorphic features is difficult to constrain.

Surface process models that focus on some or all of the landscape can be used to derive quantitative estimates of how topographic change relates to erosion history and geomorphic features. Previous work linking topography and apatite fission track (AFT) data from the southwest coast indicated the existence of a pre-breakup drainage divide similar to the present-day divide in this area (Van Der Beek et al., 2002). Block landscape models showed that continent-scale tilting during early Late Cretaceous uplift was necessary to reproduce the major pulse of sediment to the marine basins on the west coast at that time (Braun et al., 2014). Additional modeling of a generic continent subjected to a propagating wave of dynamic topography argued that the modeled sedimentary architecture was consistent with Cretaceous sedimentary archives from southern Africa (Ding et al., 2019). Modeling efforts focused on river profile shape have taken this approach a step further by comparing modeled and observed river profiles to invert for uplift histories that suggest that the high topography was developed in the last 30–40 Ma (Paul et al., 2014; Roberts & White, 2010; Rudge et al., 2015). This method allows the systematic exploration of a wide range of uplift parameters, but the absolute timing of the uplift histories it yields depends on an assumed value for rock erodibility, which is difficult to constrain. All of these methods have only focused on one main piece of the erosion history or landscape, yielding important insights into aspects of the southern African topographic history but leading to incomplete and sometimes conflicting results between modeling approaches.

Here we aim to take advantage of the many data sets quantifying the erosion history of southern Africa and combine them with topographic metrics to explore how much uplift occurred during each of the three proposed periods of plateau development using landscape evolution model inversions. Through the integration of thermochronology, marine sediment flux volumes, and topography we aim to quantify the surface uplift histories that are most compatible with all the observations. To do this, we use a highly efficient forward landscape evolution model, FastScape (Braun & Willett, 2013), to predict erosion and topography from a wide range of uplift histories and erosional parameters. Model outputs are directly compared with observations, and we use an inversion optimization scheme to isolate the uplift histories that best match the data. Resulting good fit histories give quantitative estimates of uplift magnitudes and rates through time that are compared to proposed geodynamic mechanisms for uplift.

2. Background

2.1. Geomorphic and Geologic Setting

Southern Africa forms a broad (>1,200 km wide) plateau with the highest elevations around the rim of the plateau forming what has been termed the “great escarpment” (Figure 1). The escarpment sits generally 100–200 km inboard of the coast and is often interpreted as a resulting from the retreat of a set of flexural rift shoulders (e.g., Braun, 2018; Gilchrist et al., 1994; ten Brink & Stern, 1992) that separates the higher relief, more heavily eroded coastal plains from the plateau interior. At present, the interior of the plateau is almost

entirely drained by the west-draining Orange River system. Evidence from much higher sediment flux rates on the west coast than the south and east coasts (e.g., Baby et al., 2020; Guillocheau et al., 2012; Tinker et al., 2008a) and the locations of detrital diamond on the west coast sourced from the Kaapvaal Craton (Bluck et al., 2005; Nakashole et al., 2018; Phillips & Harris, 2009; Phillips et al., 2018) show that the plateau has been west-draining since Gondwana breakup. Drainage reconstructions suggest some reorganization of plateau drainage since the Cretaceous, but most suggest the dominance of large, west-draining river systems (M. C. J. de Wit, 1999; Dingle & Hendry, 1984; Partridge & Maud, 1987; Stevenson & McMillan, 2004).

Geologically, southern Africa is a continental shield composed of dominantly Precambrian lithosphere. The Archean Kaapvaal and Zimbabwe cratons are sutured by the Archean to Paleoproterozoic Limpopo Belt and surrounded by several other Proterozoic mobile belts (Figure 1). This crystalline basement is overlain by several locally preserved Precambrian sedimentary and volcanic sequences. In the south, the Paleozoic Cape Supergroup was folded into the Cape Fold Belt (~275 to ~250 Ma, Hansma et al., 2016). Much of the Cape Fold Belt consists of quartzites that are resistant to erosion (Scharf et al., 2013). As a whole these Precambrian and Paleozoic rock units are relatively resistant to erosion.

The Karoo Supergroup was deposited from ~300 to ~180 Ma. It once covered much of southern Africa with substantial thickness still preserved today (Figure 1). Deposition was partly contemporaneous with the development of the Cape Fold Belt and in places they are deformed by this event (Linol & De Wit, 2016). These siliciclastic rocks were deposited either in a foreland basin related to this orogeny (Catuneanu et al., 2005) or due to dynamic subsidence induced by subduction to the south (Pysklywec & Mitrovica, 1999). Sedimentation terminated with the eruption of the ~183 Ma basalts of the Karoo Large Igneous Province (LIP) (Duncan et al., 1997; Jourdan et al., 2008). In addition to the basalts, an extensive network of dolerite sills was emplaced within the entire Karoo sequence, concurrent with eruption of the basalts at the surface (Svensen et al., 2012). The maximum preserved thickness of the Karoo Supergroup is up to 6 km (Scheiber-Enslin et al., 2015), with up to 1.7 km of basalt preserved in the Lesotho remnant (Marsh et al., 1997). The Karoo sequence is much less resistant to erosion than the underlying Precambrian rocks and Cape Fold Belt (e.g., Braun et al., 2014).

Post-Karoo units include the relatively thin poorly dated Cenozoic Kalahari Group rocks and sediments in the north. The Kalahari Group reaches a maximum thickness of 450 m but is dominantly <200 m thick (Haddon & McCarthy, 2005). Cretaceous and younger igneous rocks include the ~132 Ma (Renne et al., 1996) Etendeka LIP in western Namibia and South Africa, and many Cambrian to Paleogene kimberlites. Two major pulses of kimberlite magmatism occurred during the Jurassic and Cretaceous, with pulses peaking at ~90 Ma and ~120 Ma (Jelsma et al., 2004).

2.2. Constraints on the Erosion History of Southern Africa

2.2.1. Offshore Constraints From Stratigraphy

Terrigenous sedimentary flux shed off the continent has been quantified for the western and southern margins of southern Africa based on seismic lines and borehole data (Baby, Guillocheau, Boulogne, et al., 2018; Baby et al., 2020; Baby, Guillocheau, Morin, et al., 2018; Guillocheau et al., 2012; Rouby et al., 2009; Tinker et al., 2008a). This includes quantifying the siliciclastic component by correcting for in-situ carbonate production and porosity (Baby, Guillocheau, Boulogne, et al., 2018; Baby et al., 2020; Baby, Guillocheau, Morin, et al., 2018; Guillocheau et al., 2012). The Orange River presently drains most of the southern African Plateau, such that much of the sediment removed from the landscape is deposited in the Orange River Basin (Figure 2). There is only limited onshore sediment storage in the Orange River drainage, with no large continental basins, making this a good location for source-to-sink studies. The sedimentary sequence in the Orange Basin records two periods of high sedimentary volumes and accumulation rates in Early (~150–130 Ma) and Late (93.5–81 Ma) Cretaceous times bracketing an interval of low accumulation in the mid-Cretaceous (130–100 Ma, Baby, Guillocheau, Morin, et al., 2018; Guillocheau et al., 2012). The Cenozoic period is characterized by low sediment volumes and accumulation rates with a slight increase in rates in the southern part of the margin since 11 Ma (Figure 2, Baby, Guillocheau, Morin, et al., 2018; Guillocheau et al., 2012). The basins off the southern and eastern coasts show much lower volumes of sediment but with

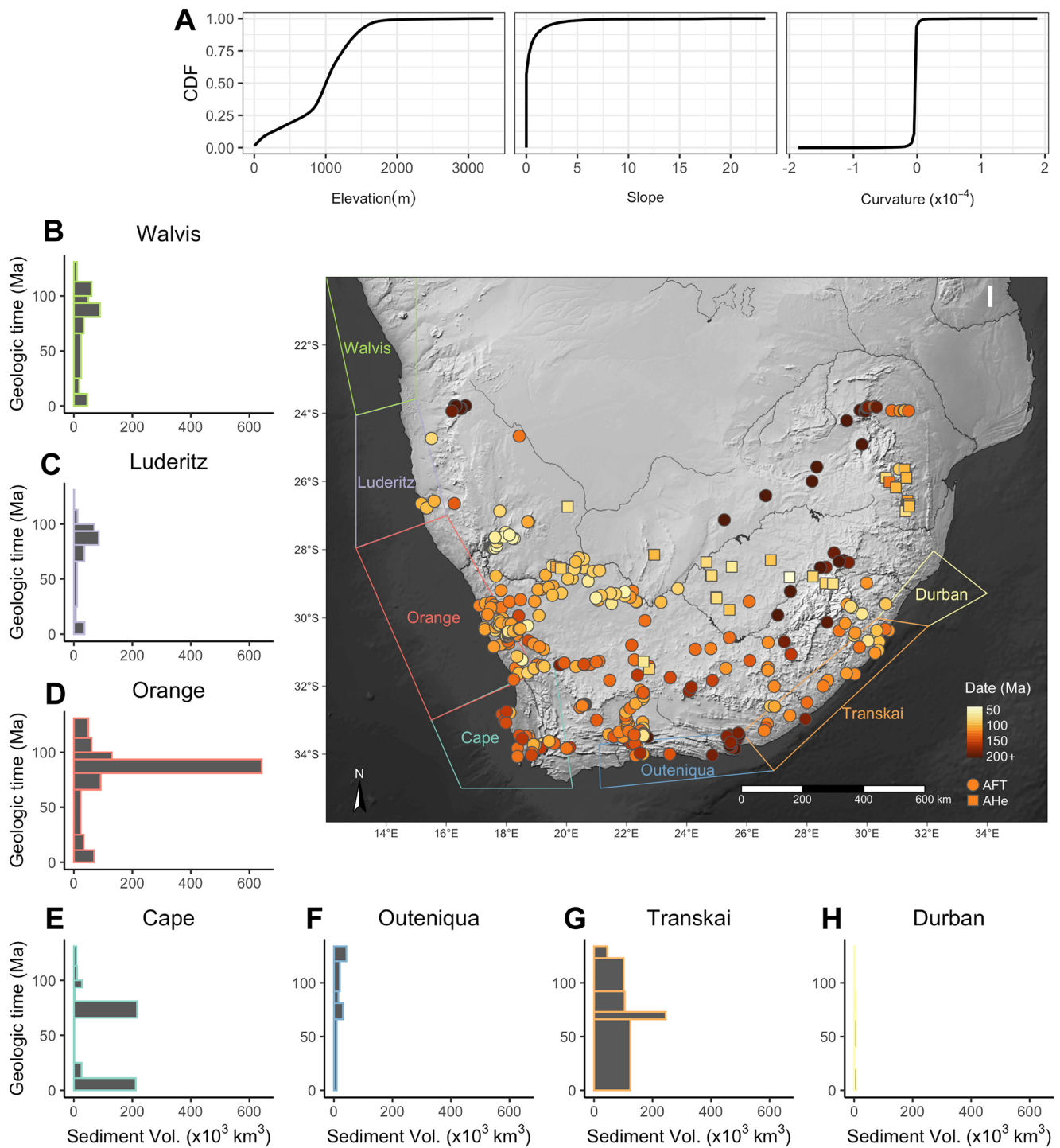


Figure 2. Data included in inversion modeling. (a) Cumulative density functions (CDF) for present day elevation, slope, and curvature from southern Africa derived from the ETOPO1 data set (Amante & Eakins, 2009). (b–h) Sediment volumes deposited over time in the marine basins surrounding southern Africa (Baby et al., 2020). (i) Shaded relief map showing the locations of low temperature thermochronology dates with color denoting age (Brown, 1992; Brown et al., 1990, 2002, 2014; M. C. J. De Wit, 1988; Flowers & Schoene, 2010; Green et al., 2017; Kounov et al., 2009, 2013; Raab, 2001; Raab et al., 2002; Stanley & Flowers, 2020; Stanley et al., 2013, 2015; Tinker et al., 2008b; Wildman et al., 2015, 2016, 2017). AFT, Apatite Fission Track, AHe, Apatite (U-Th)/He. Outlines of basins used in landscape modeling shown in colored boxes (see Baby et al., 2020, for full extent of marine basins used to compile sediment volumes).

a similar pattern: high accumulation rates in the Early and Late Cretaceous, followed by much lower rates in the Cenozoic (Figure 2, Baby, Guillocheau, Boulogne, et al., 2018; Braun et al., 2014; Tinker et al., 2008a).

The sedimentary records of both the Indian (Baby, Guillocheau, Boulogne, et al., 2018) and Atlantic (Baby, Guillocheau, Morin, et al., 2018) margins show evidence for two phases of uplift at around 93–70 Ma and 25–15 Ma. Evidence comes from margin tilting and truncation, forced regressive wedges recording a relative sea-level fall with an amplitude higher than 100 m/Ma and incised valleys (see Baby, Guillocheau, Boulogne, et al., 2018 for a discussion). The stratigraphic record (Baby, Guillocheau, Boulogne, et al., 2018; Baby, Guillocheau, Morin, et al., 2018; Braun et al., 2014) indicates margin uplift and tilting of the Southern African Plateau, starting in the east (Durban Margin) at 93 Ma and ending in the west (Orange to Olifant Margin) at 81–70 Ma. After a period of no deformation (70–35 Ma), significant uplift started again along the Durban Margin (25–15 Ma) and earlier (35 Ma) further northeast (Ponte et al., 2019).

2.2.2. Onshore Constraints From Thermochronology

Apatite fission track (AFT) and (U-Th)/He (AHe) thermochronology are dating techniques that track the cooling and heating of rocks through the upper ~1–6 km of crust and can be used to constrain the long-term burial and erosion of a region. AHe is sensitive to temperatures of ~30–90°C (Farley, 2000; Flowers et al., 2009; Shuster et al., 2006). Assuming a 15°C surface temperature typical cratonic geothermal gradient of 20°C/km, AHe can be used to detect erosion in the upper ~1–4 km of crust. AFT is sensitive to somewhat higher temperatures of ~60–110°C (Green et al., 1986) or ~2–5 km depth assuming the same cratonic gradient. Many studies have used low-temperature thermochronology to constrain the long-term erosion histories in southern Africa.

The majority of studies have used AFT on the high-relief eastern (Brown et al., 2002), southern (Green et al., 2017; Tinker et al., 2008b), and western (Gallagher & Brown, 1999b; Kounov et al., 2009, 2013; Wildman et al., 2015, 2016) margins of the plateau (Figure 2). These studies show two periods of accelerated erosion in the Cretaceous, the first at ~150–120 Ma following continental breakup and the second at ~100–70 Ma. This work also suggests limited Cenozoic erosion, though Green et al. (2017) suggest an episode of burial and erosion of parts of the Southwest Cape during the Cenozoic. AHe data across the eastern plateau escarpment also detects a cooling phase at ~100 Ma and limits Cenozoic erosion to <750 m (Flowers & Schoene, 2010). AHe data across the interior of the plateau record greater spatial variability than the plateau edges with erosion migrating eastward from ~120 to <60 Ma (Stanley & Flowers, 2020; Stanley et al., 2013, 2015) and the central part of the Kaapvall Craton showing limited erosion since before the breakup of Gondwana (Wildman et al., 2017) with unreset dates near drainage divides (Figure 2). These results also suggest limited Cenozoic erosion of ~1 km or less.

Cosmogenic nuclide derived erosion rates suggest that erosion rates on both the plateau surface and the coastal plain have been slow over the last few Myr. Most erosion rates, both catchment averaged and bedrock, are <10 m/Myr (Bierman et al., 2014; Chadwick et al., 2013; Cockburn et al., 1999, 2000; Decker et al., 2013; Dirks et al., 2016; Fleming et al., 1999; Kounov et al., 2007; Makhubela et al., 2019; Scharf et al., 2013), one to two orders of magnitude lower than thermochronologically derived rates for the Cretaceous. However, several studies focused around river channels suggested higher denudation rates (12–255 m/Ma) highlighting some potential landscape variability (Erlanger et al., 2012; Keen-Zebert et al., 2016).

2.2.3. Onshore Constraints From Geological Observations

Early geomorphologists described and correlated a number of geomorphic surfaces across the southern African landscape that were attributed to cycles of uplift and denudation (e.g., Dixey, 1955; King, 1942, 1950; Partridge & Maud, 1987; Partridge et al., 2010). Age assumptions for these surfaces suggest plateau uplift in the Cenozoic (Burke, 1996; Burke & Gunnell, 2008; Partridge & Maud, 1987), however such assessments and associated uplift mechanisms remain poorly dated. Surfaces in the plateau interior are mid- to Late Cretaceous in age based on cross cutting kimberlites (Baby, 2017), while pediments and wave cut platforms on the continental margins are thought to be younger (<25 Ma, Baby, 2017). In the lower Orange River Valley, these surfaces and alluvial terraces were used to argue for >200 m of uplift of this region in the Cenozoic (Dauteuil et al., 2015).

Table 2
Variable Parameters in Inversion Model, Their Ranges, and Their Values From the Best Fit Models From the Cretaceous and Hybrid Scenarios

Variable parameter	Units	Value range	Hybrid early best fit	Hybrid late best fit	Cretaceous low best fit	Cretaceous high best fit
K_f : Erosivity	$m^{0.2}/yr$	10^{-7} – 10^{-4}	3.11×10^{-6}	9.22×10^{-5}	7.21×10^{-5}	2.15×10^{-7}
ϵ_c : Threshold for erosion	m/yr	10^{-5} – 10^{-2}	18.9×10^{-5}	2.37×10^{-3}	9.076×10^{-3}	1.08×10^{-5}
T_{max} : Temperature at base of 120 km thick model lithosphere	°C	2,400–5,000	4,937	4,601	4,934	4,962
R_k : Ratio of thermal diffusivity between 2 km thick Karoo sedimentary cover and underlying basement		0.3–1	0.458	0.313	0.392	0.306
R_D : Ratio between volume of material eroded and volume of material deposited in the marine basins		1–5	2.43	4.91	3.20	1.91
h_0 : height of initial base plateau in first time step	m	200–2,000	259.9	222.0	205.3	201.0
t_{init} : Geologic time when uplift and tilting initiates in the east	Ma	120–75	89.83	99.08	97.49	98.605
h_{tilt} : Magnitude of Cretaceous tilting	m	200–3,000	641.2	687.6	1,293	2,486
t_{tilt} : Duration of time continent remains tilted before uplift initiates in the west	Myr	5–35	8.370	11.63	6.109	15.29
t_{block} : Geologic time of second phase of block uplift	Ma	40–0	29.28	11.1	33.20	38.48
h_{block} : amount: magnitude of second phase of uplift	m	0–2,000	663.7	751.6	1.272	4.766

Reconstructed thicknesses of the Karoo Supergroup can help constrain total erosion magnitudes since ~ 180 Ma. The amount of material denuded across the main Karoo Basin on the plateau surface is estimated at ~ 0.5 – 3 km of material (Hanson et al., 2009), but varies based on location, reconstruction method, and the proposed thinning rates for the units (Hanson et al., 2009; Hawthorne, 1975; Johnson et al., 1996). Similar efforts at reconstructing stratigraphic thicknesses on the southern margin suggest a range of erosional magnitudes from 4 to 11 km (Richardson et al., 2017). Crater lake sediments preserved in the ~ 75 – 65 Ma kimberlite pipes in the western Plateau suggest that this area has seen very limited erosion since that time (Moore & Verwoerd, 1985; Scholtz, 1985; Smith, 1986).

3. Modeling Methods

3.1. Modeling Strategy and Data

We seek to test the three proposed intervals for the rise of the southern African plateau using the breadth of erosion and sedimentation data that is now available here. To do this we use a large-scale landscape evolution model to predict thermochronology dates, sediment fluxes, and topography from different uplift inputs. We explore which parameter sets fit the observations best using inversion methods combined with an optimization algorithm. The parameter space is too large to sample in its entirety, so we use the neighborhood algorithm (NA, for full description see Sambridge, 1999), to guide a total of 500,000 model runs varying 11 parameters (Table 2). We then compare model results to three different types of observations: thermochronology dates, marine sediment flux volumes, and topographic metrics.

The thermochronology data include 362 published AFT dates from Precambrian basement and Karoo sedimentary rocks (Belton & Raab, 2010; Brown, 1992; Brown et al., 1990, 2002, 2014; Green et al., 2017; Kounov et al., 2009, 2013; Raab, 2001; Raab et al., 2002; Tinker et al., 2008b; Wildman et al., 2015, 2016, 2017) and 29 average AHe dates from Precambrian basement, Cretaceous kimberlites, and mafic rock samples (Flowers & Schoene, 2010; Stanley & Flowers, 2020; Stanley et al., 2013, 2015). The full data table can be found in the supplementary materials Table S1. Samples span from across southern Africa between 23.5° S and 36° S and cover both the coastal margins and the plateau interior, though there is more data from the coastal regions (Figure 2).

The sediment flux data come from volume estimates of terrestrially derived sediment in seven marine basins on the western and southern coasts of southern Africa (Figure 2). These volumes were calculated from seismic data and borehole observations (Baby, Guillocheau, Boulogne, et al., 2018; Baby et al., 2020; Baby,

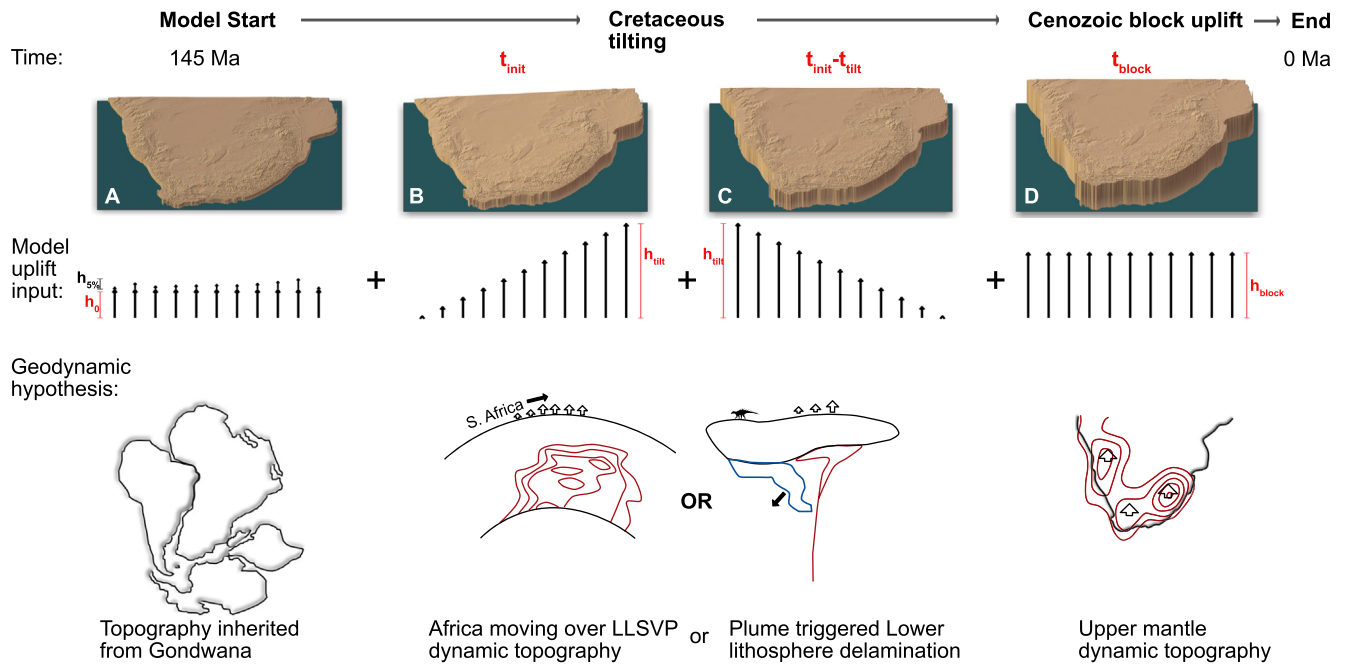


Figure 3. Schematic diagram of uplift imposed on the model through time. Parameters in red are variable in the inversion (Table 2), while black are fixed (Table 3). During the first time step (a), an uplift of height h_0 plus 5% of present day topography is imposed. At time t_{init} (b) a linear tilt is imposed as a vertical stress at the base of the model, and after t_{tilt} an opposing tilt to flatten the continent is imposed (c). Finally, at t_{block} a vertical stress at the base of the model is imposed to create an additional height of h_{block} (d). It should be noted that uplifts that are imposed as a vertical stress may produce magnitudes of rock uplift and erosion higher than the uplift amount due to isostatic feedback. Times are shown in geologic time. Bottom panels show cartoons depicting geodynamic hypotheses being tested at each stage. Uplift at model start represents topography inherited from prior to Gondwana breakup. Cretaceous tilting could be due to movement of Africa over a dynamic topography high due to the lower mantle LLSVP or lower lithosphere delamination triggered by kimberlite magmatism. Cenozoic uplift could be due to upper mantle buoyancy, perhaps denoted by present day free air gravity anomaly highs (after Winterbourne et al., 2009). See Table 1 for more explanation.

Guillocheau, Morin, et al., 2018). Tables of the sedimentary volumes and basins are located in the supplement (Table S2).

The present-day topography is derived from the ETOPO1 one arc-minute global topographic and bathymetric data set (Amante & Eakins, 2009). Topography ranges from sea level to 3,376 m elevation, with a median elevation of 1,037 m (Figure 2).

3.2. Forward Model Setup

3.2.1. Model Setup and Uplift

The landscape model runs from 145 Ma to present with timesteps of 1 Myr. Parameterization of the model allows for topographic development corresponding to the three main phases that have been proposed for uplift of the Kalahari Plateau: (a) initial topography that represents topography formed prior to Gondwana breakup, (b) a phase of uplift and continental tilting in the Cretaceous, and (c) a phase of block uplift in the Cenozoic (Figure 3, Table 1). The magnitude, time, and combination of uplift during these phases vary widely within the inversion (Table 2).

The initial topography represents any plateau development that occurred prior to or during Gondwana breakup. All models start with 5% of today's topography (0–150 m) to seed the drainage basins. This is then uplifted uniformly within the first timestep by an additional plateau height h_0 which induces a flexural response at the margins, mimicking rifted margin topography (Figure 3, Tables 2 and 3). We seed the drainage basins to reflect the current basins because the geologic record indicates that large, west-draining river systems have been persistent in southern Africa since Gondwana breakup (e.g., M. C. J. de Wit, 1999). This westward draining nature of the plateau is important for determining where sediment is routed, and we

Table 3
Fixed Parameter Values and Justification

Fixed parameter	Units	Value	Justification
n : Slope exponent in stream power law		1	Literature values range from 0 to 4, $n = 1$ chosen for numerical efficiency.
m : Drainage area exponent in stream power law		0.4	Literature values range from 0 to 2, ratio of m/n derived from slope-area relationships in natural landscapes ranges from 0.35-0.6 (Kirby & Whipple, 2012; Whipple, 2004; Whipple & Tucker, 1999).
T_e : Elastic thickness	km	20	Effective elastic thickness estimates for southern Africa range from ~10 km near the coasts to >70 km in the cratonic interior (Doucouré et al., 1996; Pérez-Gussinyé et al., 2009). We have chosen a value representative of the continental margins because flexural effects are most important to the landscape there.
t_{up} : time period over which each dynamic uplift stage is imposed	Myr	5	It is geologically unreasonable for uplift to occur instantaneously.
Karoo layer thickness	km	2	Soft layer representing sediments and basalt overlying basement that can also have different thermal diffusivity.
Karoo layer erosivity	$m^{0.2}/yr$	$30(K_f)$	Braun et al. (2014) demonstrated that a soft layer was important for reproducing the Cretaceous sediment pulse.
E : Young's modulus	GPa	1×10^{11}	
ν : Poisson's ratio		0.25	
ρ_c : crustal density	kg/m^3	2,750	
ρ_a : asthenospheric density	kg/m^3	3,300	
κ : thermal diffusivity of basement	m^2/yr	25	
Lithospheric thickness	km	120	
Kinetic model for apatite fission track annealing			Crowley et al. (1991) (Durango)
Kinetic model for He diffusion in apatite			Farley (2000)

found that such a drainage geometry was difficult to create spontaneously. The features of the landscape at 145 Ma are not known but a low relief landscape is a reasonable assumption given that much of the landscape was covered with the Karroo Basin and flood basalts. 5% of today's topography is sufficient to setup a west draining geometry, but low enough magnitude that it can be easily disrupted by uplift imposed later in the model.

In the Cretaceous, we impose a phase of continental tilting that initiates in the east at a time t_{init} . It tilts linearly to the west, reaching a maximum height of h_{tilt} 5 Myr after uplift initiates (Figure 3, Tables 2 and 3). The continent remains tilted for a duration of time t_{tilt} , at which point uplift begins in the west reaching the same height and a flat uplift after 5 Myr (Figure 3). The continent then retains this dynamic uplift for the rest of the model run. We chose this continental tilting shape for the Cretaceous uplift phase because previous modeling (Braun et al., 2014) showed that this was important for producing the large pulse of sediment observed in the basins off the west coast. Additionally, we found that the tilting geometry was best for preserving a large, west-draining drainage basin geometry while many other uplift shapes we tested disrupted this drainage network.

Finally, in the Cenozoic, at a time t_{block} , a phase of dynamic block/uniform uplift is imposed with a magnitude h_{block} (Figure 3, Table 2). Once its maximum value is reached, the uplift is maintained until the end of the model run. The model domain ranges from 20°S to 35°S and 12°W to 36°W and is discretized on a 1 arc-second grid for ease of comparison with the ETOPO1-derived present-day topography. For simplicity, base level remains fixed at the present-day coastlines throughout the model run, and the northern boundary

is a reflective, no-flux boundary. The model starts with a uniform, 2 km thick softer layer representing the Karoo sedimentary rocks and basalts overlying a harder layer representing the Precambrian basement.

3.2.2. The Landscape Evolution Model

The landscape evolution model solves the basic stream power model for bedrock river incision (Howard & Kerby, 1983),

$$\frac{\partial h}{\partial t} = U - \max(0, K_f S^n A^m - \varepsilon_c) \quad (1)$$

where h is the height of the topography, t is time, U is uplift rate, S is slope, A is drainage area, K_f is the erosion efficiency scaling parameter, m and n are constants, and ε_c is an erosion threshold. Equation 1 is solved by the FastScape algorithm (Braun & Willett, 2013). FastScape is a very efficient, first order, implicit, finite difference algorithm for solving the stream power equation that makes it possible to run many forward models rapidly enough to complete inversions. The values of K_f , m , and n are not well constrained but depend dominantly on climate, lithology, and hydrology. We use standard values of $n = 1$ and $m = 0.4$ and allow K_f to vary over several orders of magnitude between 10^{-7} and 10^{-4} m^{0.2}/yr. K_f for the 2 km thick soft layer is 30 times the value of K_f for the underlying material (Table 3). All parameter values and their justification can be found in Tables 2 and 3 (see Croissant & Braun, 2014, for a more thorough discussion of the values of the erosional parameters). The introduction of the erosion threshold, ε_c with units of m/yr, implies that some base level of stream power is needed to erode the landscape. ε_c is also allowed to vary over several orders of magnitude (Table 2). Flow is routed using a D8 grid connectivity, and local depressions are filled using the algorithm of Cordonnier et al. (2019). All water and sediment is routed out to the marine basins for computational efficiency and because onshore sediment storage is limited at the scale of our model. The Kalahari Basin, limited to the northern part of our model (Figure 1), represents the only onshore depocenter and based on published isopachs (Haddon & McCarthy, 2005) the Kalahari deposits have a maximum volume of 6% of the volume of terrigenous sediments in the offshore basins (Baby et al., 2020). We do not include a model for hillslope processes because they cannot be adequately represented at the scale of our model (i.e., grid resolution of 1×1 km). This is a highly simplified description of erosion, and unlikely to capture the true complexity of erosion processes across the southern African landscape but it is sufficient for comparison at the scale of our model and data types we have incorporated. This process model is applied at every time step of the imposed uplift history, starting with 5% of today's topography plus the uplift h_0 in the first time step.

We compute the flux of sediment leaving the continent along various sections of the continental margin corresponding to major depocenters as shown in Figure 2. We introduce a deposition ratio, R_D , which multiplies the eroded flux to produce a depositional flux into the marginal basins that is compared to observed fluxes. This ratio accounts for imbalances in the amount of material eroded and deposited that could be caused by processes such as chemical denudation or transport of material away from the depocenter.

The landscape model is coupled to an isostatic model that includes flexure of a thin elastic plate:

$$D \frac{\partial^4 U}{\partial x^4} + D \frac{\partial^4 U}{\partial y^4} + D \frac{\partial^4 U}{\partial x^2 \partial y^2} = \Delta \rho g U + \rho_c g \Delta h + \sigma_{DT} \quad (2)$$

where D is the flexural rigidity, ρ_c is the crustal density, $\Delta \rho$ is the density difference between ρ_c and the asthenospheric density, and σ_{DT} is an imposed basal stress that could represent viscous stress from mantle flow or an isostatic response from delamination of the lithospheric mantle. D is related to Young's modulus (E), the elastic thickness (T_e), and Poisson's ratio (ν):

$$D = \frac{ET_e^3}{12(1 - \nu^2)} \quad (3)$$

The flexure equation is solved using the Fast Fourier Transform method in the spectral domain on a fixed grid using methods similar to Nunn and Aires (1988).

Uplift is imposed as a vertical stress field along the base of the lithosphere through the flexural-isostatic model (Equation 2) as σ_{DT} , where σ_{DT} is the stress required to lift the surface topography to the imposed height. In this setup, surface erosion results in the rebound of surface topography such that the weight of the surface topography remains equal to the basal load. This can continue until the deflection at the base of the crust is sufficient to balance the load.

3.2.3. Thermal Model

A 1D thermal model is coupled to the landscape model to predict cooling dates from the modeled erosion history for comparison with the observed data. For each location where a predicted cooling date is needed, the erosion rate is stored for each time step and used to generate an exhumation history at the end of the model run. These erosion rates are then used to solve the 1D heat equation:

$$\frac{\partial T}{\partial t} + \dot{E} \frac{\partial T}{\partial z} = \kappa \frac{\partial^2 T}{\partial z^2} \quad (4)$$

where \dot{E} is the erosion rate and κ is the thermal diffusivity. The implementation in the model also allows for layers with differing thermal diffusivities, and their thicknesses are adjusted throughout the model run to account for their erosion. The 1D model yields spatially and temporally variable thermal gradients depending on local erosion rate and preservation/erosion of layers with differing thermal parameters but does not compute lateral motion of heat. The solution is used to compute time-temperature paths and predict dates for thermochronological systems (Braun et al., 2006). To account for the fact that some of the observed thermochronology dates are older than the length of the model run, the time temperature path is extended isothermally from 145 Ma to an age limit, set at 300 Ma for most samples (older than 95% of observed AFT dates). If a sample's igneous age is younger than 300 Ma the igneous ages used as the age limit (Table S1).

The temperature at top and base of the model is fixed, with the surface at 15°C and T_{\max} at the base of a 120 km thick lithosphere which correspond to surface geothermal gradients between ~20 and 42°C/km. We do not directly account for heat production in the crust and lithosphere and instead fix the base of the model to produce an initial, linear, diffusive geothermal gradient over this range that encompasses what is currently observed in southern Africa (e.g., Macgregor, 2020). Because the base of the model is the base of the lithosphere, this results in unreasonably high lithosphere-asthenosphere boundary temperatures (T_{\max} , Table 2). We are not asserting that these temperatures are correct but this sets up a reasonable thermal structure in the upper crust that can be constrained by our data. The thermal diffusivity of the soft layer at the top of the model representing the Karoo Supergroup can vary from 0.3 to 1 times the basement thermal diffusivity, R_K , allowing for a thermal blanketing effect (Tables 2 and 3).

3.3. Inversion Methods

We use the NA optimization (Sambridge, 1999) to guide the sampling of the large parameter space. At the start of the inversion, 50,000 random sets of parameters are selected from within the specified ranges (Table 2), and a forward model is run with each parameter set. For each model, a misfit that measures how well the predicted values match the observed values is calculated. For each subsequent iteration of 1,000 runs, the NA preferentially samples from areas of the parameter space with lower misfit values, while still casting a wide net (see Sambridge, 1999, for details).

The construction of a misfit function that can assign a single numerical value of how well each forward model fits the observations is central to the inversion method. However, combining assessments of different data types is nontrivial. We first compute an individual misfit for each separate data type, and then we combine these into a single misfit value for the model run.

For the topographic metrics, the misfit is calculated by comparing the cumulative distribution functions (CDFs) of the model-predicted and observed present-day topography. We compare the distributions rather than directly comparing the topography because it is unlikely that the model will replicate specific features of the model (such as exact locations of valleys and mountain tops) but should be able to replicate broader characteristics of the topography. The comparison is made using the Kolmogorov-Smirnov (KS) statistic which measures the distance between the predicted and observed distribution, yielding a value between 0

(for identical distributions) and 1 (for distributions that do not overlap). We calculate three individual misfits, M_{height} , M_{slope} , and M_{curve} that are the KS statistic for the comparison between the predicted and observed topographic height, slope, and curvature distributions, respectively.

Terrigenous sediment flux volumes have been calculated for a number of time periods in seven basins for a total of 50 volumes (Baby, Guillocheau, Boulogne, et al., 2018; Baby et al., 2020; Baby, Guillocheau, Morin, et al., 2018; Figure 2, Table S2). If N is the total number of volume calculations, the misfit for the flux, M_{flux} , takes the form of the square-root of the L_2 -norm of the weighted difference between the predicted ($V_{i,\text{pred}}$) and observed ($V_{i,\text{obs}}$) volumes for the volume from each time period:

$$M_{\text{flux}} = \frac{1}{N} \sqrt{\sum_{i=1}^N \frac{(V_{i,\text{pred}} - V_{i,\text{obs}})^2}{\sigma_{\text{avg}}^2}} \quad (5)$$

where σ_{avg} is the average uncertainty across all the flux calculations ($13.7 \times 10^{12} \text{ m}^3$). M_{flux} can range from 0, for V_{pred} equal to V_{obs} , to very large when V_{pred} is very different from V_{obs} . Values of $M_{\text{flux}} < 1$ indicate that the predicted values match the observed values within the average uncertainty.

The misfit for the thermochronology data, M_{thermo} , takes a similar form to the flux misfit:

$$M_{\text{thermo}} = \frac{1}{N} \sqrt{\sum_{i=1}^N \frac{(a_{i,\text{pred}} - a_{i,\text{obs}})^2}{\sigma_{i,\text{obs}}^2}} \quad (6)$$

where $a_{i,\text{pred}}$ is the predicted thermochronologic date for each location from the model run, $a_{i,\text{obs}}$ is the observed thermochronologic date at that location, and $\sigma_{i,\text{obs}}$ is the 1σ uncertainty associated with that date. N is the total number of thermochronologic dates included in the model, in this Case 391 (Figure 2; Table S1). For the AHe dates, $a_{i,\text{obs}}$ is the average of single grain ages for the sample and $\sigma_{i,\text{obs}}$ is the standard deviation of that mean. For each AFT date, $a_{i,\text{obs}}$ is the either the pooled age, central age, or mean age depending on what was originally published and whether the sample passed or failed the χ^2 test for homogeneity and $\sigma_{i,\text{obs}}$ is the standard error (see Table S1 for more detail). In most situations the cooling dates for low-temperature thermochronometers are expected to vary systematically with elevation (e.g., Braun, 2002). Because we cannot expect the model to reproduce the exact characteristics of the landscape, $a_{i,\text{pred}}$ is taken from the location within a 20 km radius that is closest in elevation to the observed date. M_{thermo} also ranges from 0 for an exact match between the predicted and observed dates to very large for a poor match with $M_{\text{thermo}} < 1$ indicating that the model predictions match the observations within uncertainty.

The total misfit, M , for the model run is the sum of the five individual misfits for the different data types:

$$M = M_{\text{height}} + M_{\text{slope}} + M_{\text{curve}} + M_{\text{flux}} + M_{\text{thermo}} \quad (7)$$

The misfit used to guide the parameter search in the inversion is therefore a combination of how well the model fits the combination of data types. It should be noted that the form of the misfit and how the different misfit types are weighted has a strong effect on the inversion results.

4. Results

4.1. Inversion Results

Results from topographic uplift driven inversions converge on four low-misfit parameter sets (Figure 4). Misfit values for individual forward model runs in the inversion range from 1.77 to >500 , and these four clusters of low misfit solutions contain all of the model runs with misfit values less than 2 and are differentiated by their erosional and uplift parameters (Figures 4c, 4g, 4h, and 5a–5c). In particular, we differentiate two families of low misfit models where nearly all of the topography is created during mid-Cretaceous dynamic tilting (Cretaceous Low and Cretaceous High, Figures 4c and 4f) and two families of low misfit models where topography is created during both Cretaceous tilting and Cenozoic block uplift (Hybrid Early, Hybrid Late, Figures 4c and 4f).

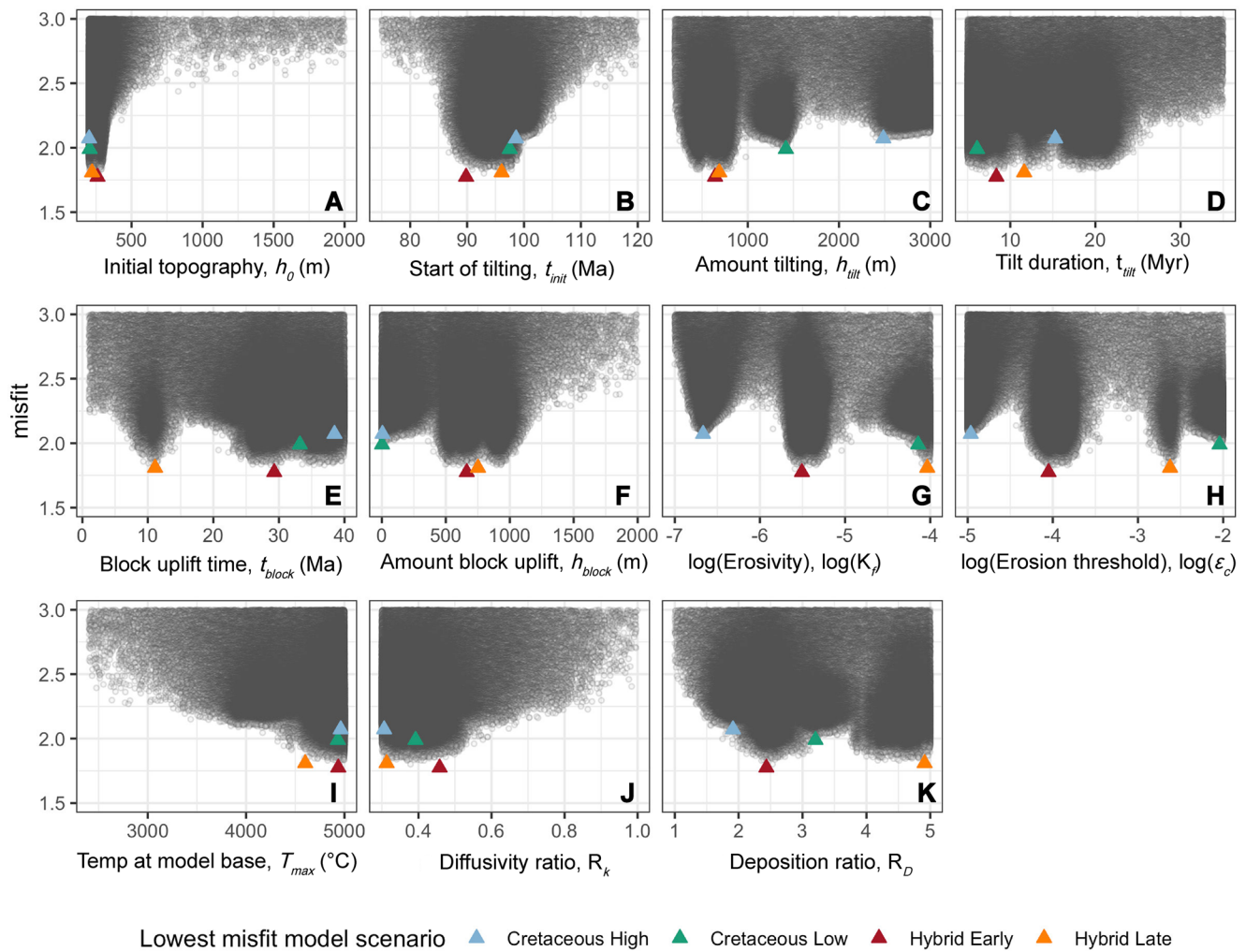


Figure 4. Plots showing the values of parameters for models with misfits < 3 . Each gray circle represents one forward model and the value for a given parameter. Each panel shows the same models but plotted with respect to one individual parameter, essentially a one-dimensional slice of the 11 dimensional parameter space. The lowest points show the parameters converging toward value(s) with better fits to the data. Blue, green, red, and orange triangles show the lowest misfit model from each of the clusters of low misfit models (the Cretaceous High, Cretaceous Low, Hybrid Early, and Hybrid Late scenarios, respectively).

All low misfit models have similar thermal parameter values, with temperatures at the base of the 120 km thick lithosphere converging at $> 4500^{\circ}\text{C}$ (Figure 4i), which would result in initial linear geothermal gradients of $> 35^{\circ}\text{C}/\text{km}$. Also, in all low misfit models the Karoo basin layer acts as a thermal blanket that is 2–3 times more insulating than the underlying basement (Figure 4j) leading to an even higher geotherm in the top 2+ km. Finally, all models converge toward a value of 2–5 for R_D which indicates that only 1/2 to 1/5 of the volume of material eroded off the surface is deposited in the basin (Figure 4k).

The families of low misfit parameter sets differ in the timing and magnitude of topographic uplift, illustrated in Figure 6 which shows the topographic uplift through time for all models run, colored by a misfit value with yellow showing the lower misfit histories. The lowest misfit models (yellow) clearly split into favored uplift patterns (Figure 6). All low misfit models have low values (~ 200 m) for h_0 , the initial plateau height added in the first timestep (Figures 4a and 6). Also, all low misfit models have some Cretaceous uplift initiating in the east between 100 and 90 Ma (Figure 4b). The four sets of low misfit models differ in the magnitude of Cretaceous and Cenozoic uplift (Figures 4c–4f and 6). The two families which we have defined as the Hybrid Scenarios have similar uplift histories and overall lower misfit values than the Cretaceous Scenarios. Both the Hybrid Early and Late scenarios have ~ 300 – 800 m of uplift during Cretaceous tilting

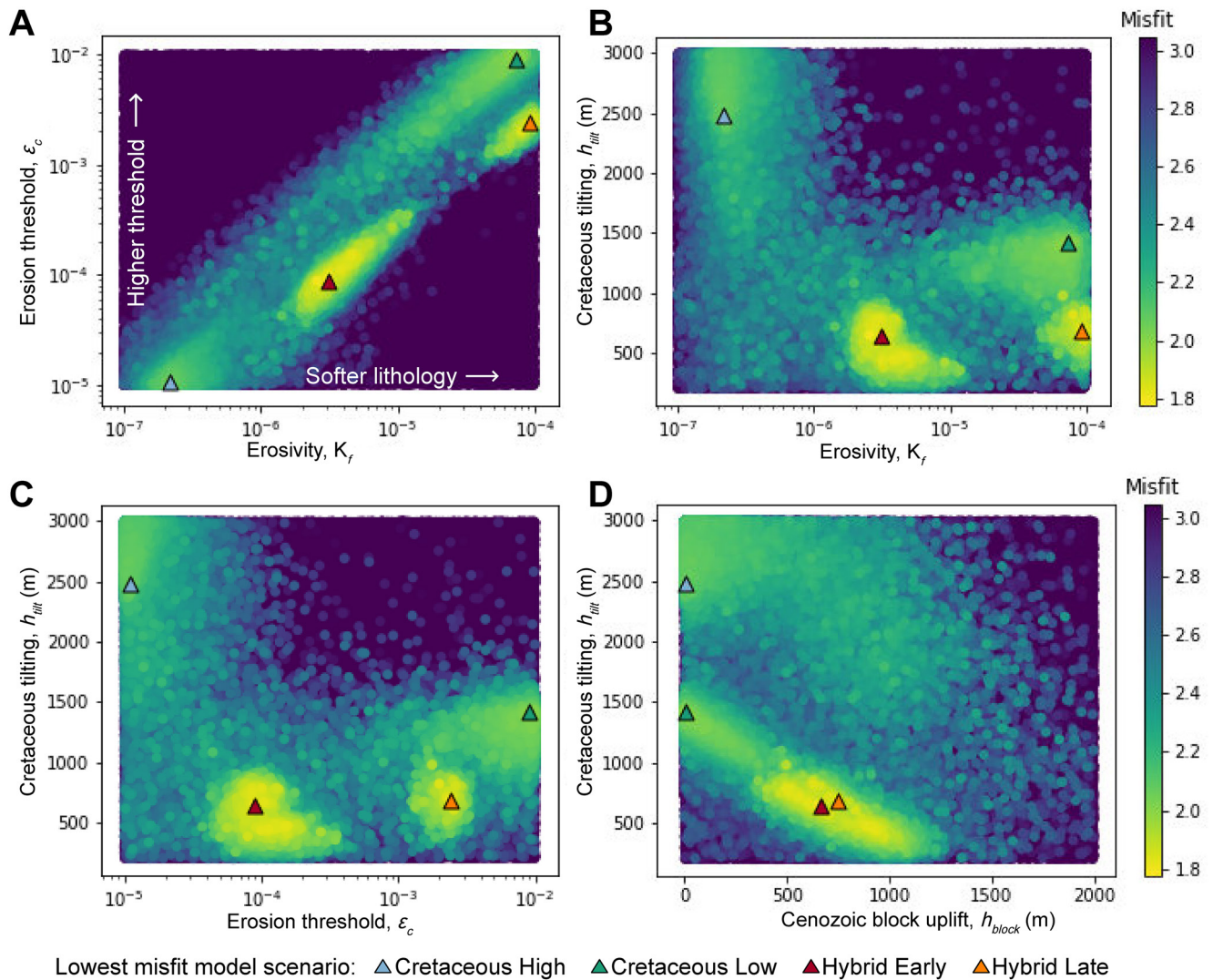


Figure 5. Plots showing the values of two parameters for models with misfits <3. Each dot represents one forward model plotted at the x, y location for the values of the given parameters colored by the misfit value for each model. Yellow dots are low misfit models. Each panel plots the same models but with respect to different parameter, essentially a two dimensional slice of the 11 dimensional parameter space highlighting the four low-misfit regions of these parameters. (a) Relationship between the erosivity and erosion threshold parameters. (b–d) Relationship between the amount of Cretaceous uplift and erosivity (B), erosion threshold (C), and amount of Cenozoic uplift (D).

(Figure 4c) and an additional ~500–1,000 m of block uplift (Figure 4f). The two Hybrid Scenarios differ in the timing of Cenozoic uplift, with Hybrid Early occurring earlier at ~40–25 Ma and Hybrid Late occurring at ~10 Ma. The Cretaceous Scenarios have nearly all of their topographic development in the Cretaceous. The Cretaceous Low Scenario has ~1,400 m of uplift in the during dynamic tilting while the Cretaceous High scenario has ~2,500 m or more of Cretaceous uplift (Figures 4c and 5). Both Cretaceous Scenarios have very low magnitudes of uplift in the second Cenozoic block uplift phase, less than a few hundred meters (Figure 4e). The Cretaceous Scenarios, in particular the Cretaceous High Scenario, have higher misfits than the Hybrid Scenarios but still form distinct minima in parameter space (Figure 5). The Cretaceous Low Scenario and both Hybrid Scenarios end with similar magnitudes of total uplift throughout the model run, on the order of 1,500–1,800 m, leading to a clear tradeoff between the amount of uplift in the Cenozoic and Cretaceous phases that is visible in a scatter plot of these parameter values and misfits (Figure 5d). Snapshots of the topography through time for the Cretaceous Low and Hybrid Late models as well as topographic profiles for all models are shown in Figure 7 (also available as Movie S1 in the supporting information).

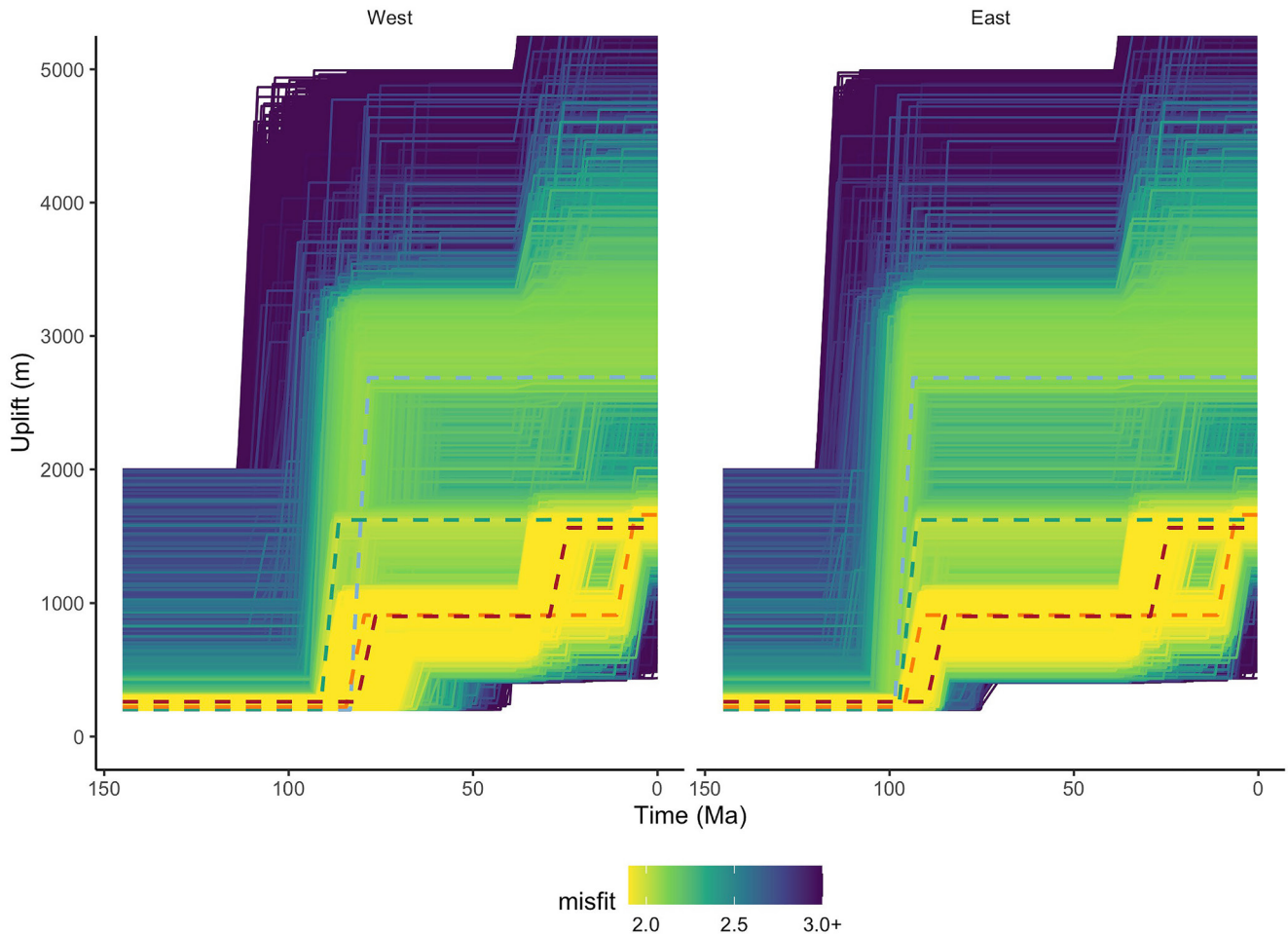


Figure 6. Uplift through time for the east edge (left panel) and west edge (right panel) of the model domain. Time is geologic time. Each line represents one forward model and is colored by the misfit value, with yellower models fitting the data better. Dashed lines show lowest misfit model for each of the clusters of low misfitting models. Light blue dashed line, Cretaceous High Scenario, green dashed line, Cretaceous Low Scenario, red dashed line, Hybrid Early Scenario, orange dashed line, Hybrid Late Scenario.

The four Scenarios also converge to different erosional parameters (Figures 4g and 4h). The two Hybrid Scenarios converge to very different absolute values of the erosional parameter, K_f , and erosional threshold, ϵ_c though with similar ratios between the two parameters (Figures 4g, 4h and 5). The Hybrid Early Scenario converges to K_f around 3×10^{-6} and ϵ_c around 1×10^{-4} , while the Hybrid Late Scenario converges to higher values (K_f around 1×10^{-4} and ϵ_c around 2×10^{-3}) indicating a more easily erodible material but a higher threshold for the Hybrid Late Scenario (Figure 5a). The Cretaceous Low Scenario converges to a similarly high erodibility as the Hybrid Late Scenario (K_f around 8×10^{-5}) but an even higher erosion threshold (around 1×10^{-2}). The Cretaceous High Scenario converges to a much harder lithology (K_f around 9×10^{-6}) but with a lower threshold (around 1×10^{-5}). There is also a tradeoff between K_f and ϵ_c that is visible in scatter plots of their parameter values and misfit (Figure 5a) with both Hybrid Scenarios and the Cretaceous High Scenario showing similar relationships between the erosivity and threshold values, and the Cretaceous Low Scenario having a higher threshold for a given erosivity.

4.2. Data-Model Comparison

The predictions from the lowest misfit model from all four scenarios are compared with the observed data in Figures 8 and 9. Overall the two families of models have a similar fit to the data, though the Hybrid Scenarios have lower misfit values and it is clear why the Cretaceous High Scenario has the highest misfit value since it does not match the topography well (Figure 9a). All models replicate the large pulse of sediment

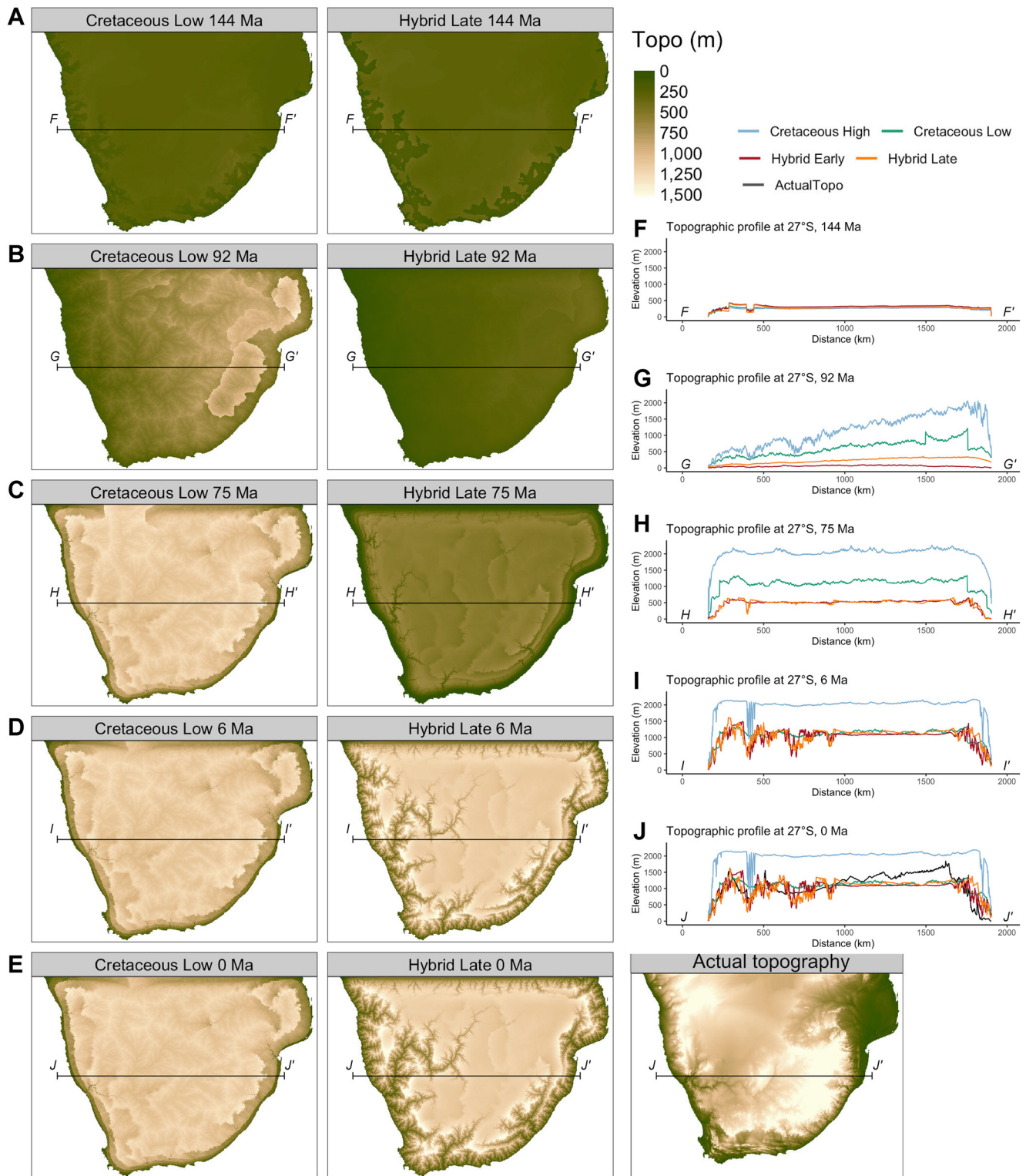


Figure 7. Topography of best fit models for the Cretaceous Low and Hybrid Scenarios through the model run with present day southern African topography shown for comparison in the last stage (a–e). Highlights just after the start of the model (a, 144 Ma), during tilting (b, 92 Ma), after of tilting (c, 75 Ma) and just after block uplift for the Hybrid Late Scenario (d, 6 Ma) to the end (e, 0 Ma). Present day southern African topography shown for comparison. Panels f–j show topographic profiles across 27°S at each time for all four low misfit model scenarios with location of profile indicated on the map figures.

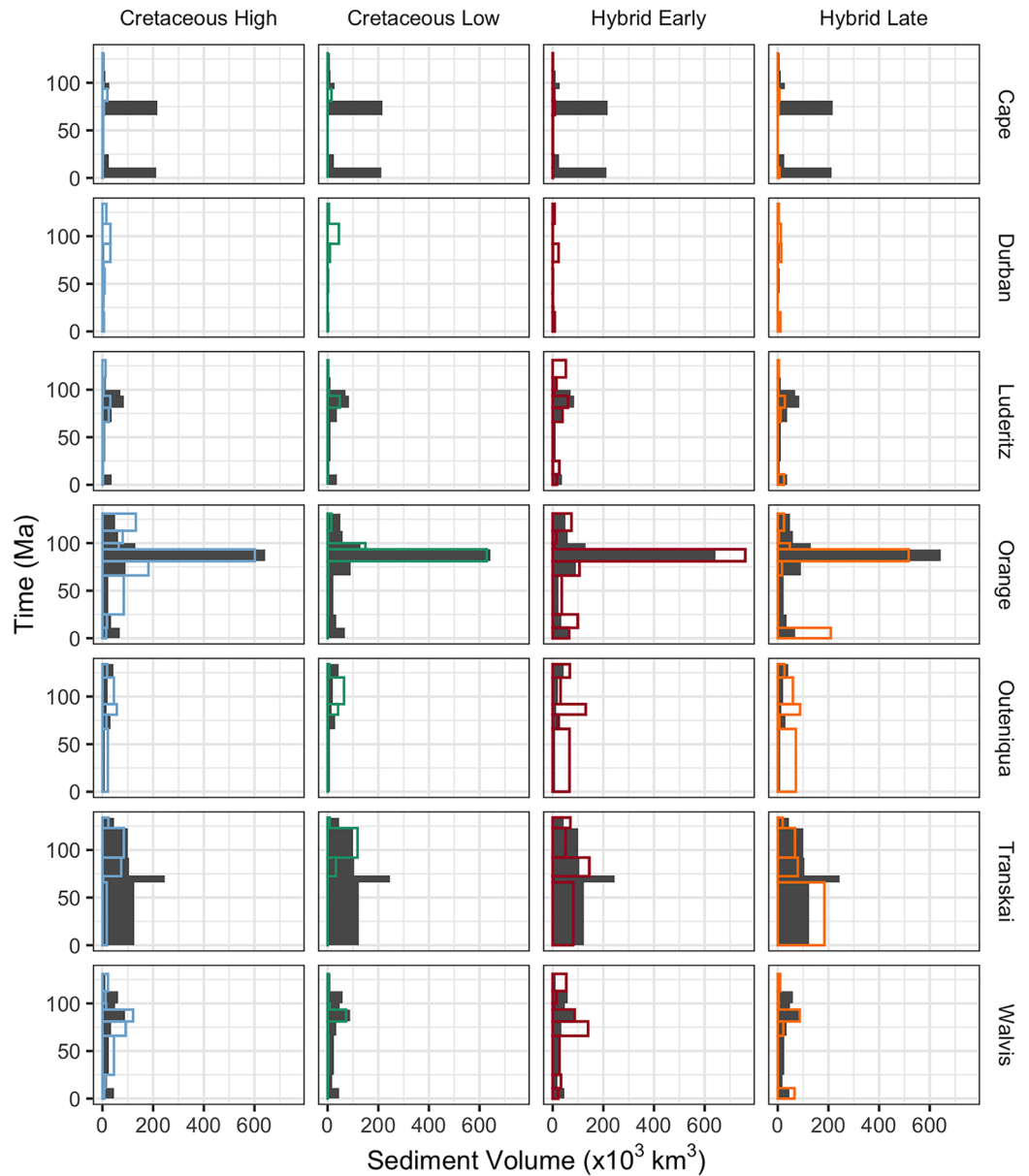


Figure 8. Sediment volumes through time from all four best fit model scenarios (colored outlines) compared with measured volumes from basins surrounding southern Africa (gray bars, Baby et al., 2020). Each column shows the results from a different model scenario while rows show different basins. See Figure 2 for locations of basins.

observed in the Orange River Basin in the Cretaceous and the overall lower fluxes observed elsewhere (Figure 8). Neither model produces the larger fluxes seen off the SW coast in the Cape Basin, and the Hybrid models do a better job of reproducing the higher fluxes in the Transkei Basin but overpredict some of the more recent volumes in the Outeniqua and Orange Basins (Figure 8). The Hybrid Scenarios and the Cretaceous Low Scenario all fit the median of the elevation distribution, but the Cretaceous High Scenario has overall higher topography than observed (Figure 9a). All models fit the median of the slope and curvature distributions reasonably well, but the Cretaceous Low scenario has the closest fit the slope and curvature distributions (Figure 9). No model is able to reproduce the complexity observed in the thermochronology data, but all are replicating a good portion of the thermochronology dates (Figure 9). The Cretaceous Scenarios predict younger dates AHe dates which is a better fit than the Hybrid Scenarios. The Cretaceous High Scenario and especially the Hybrid Late Scenario are able to reproduce some of the structure seen in

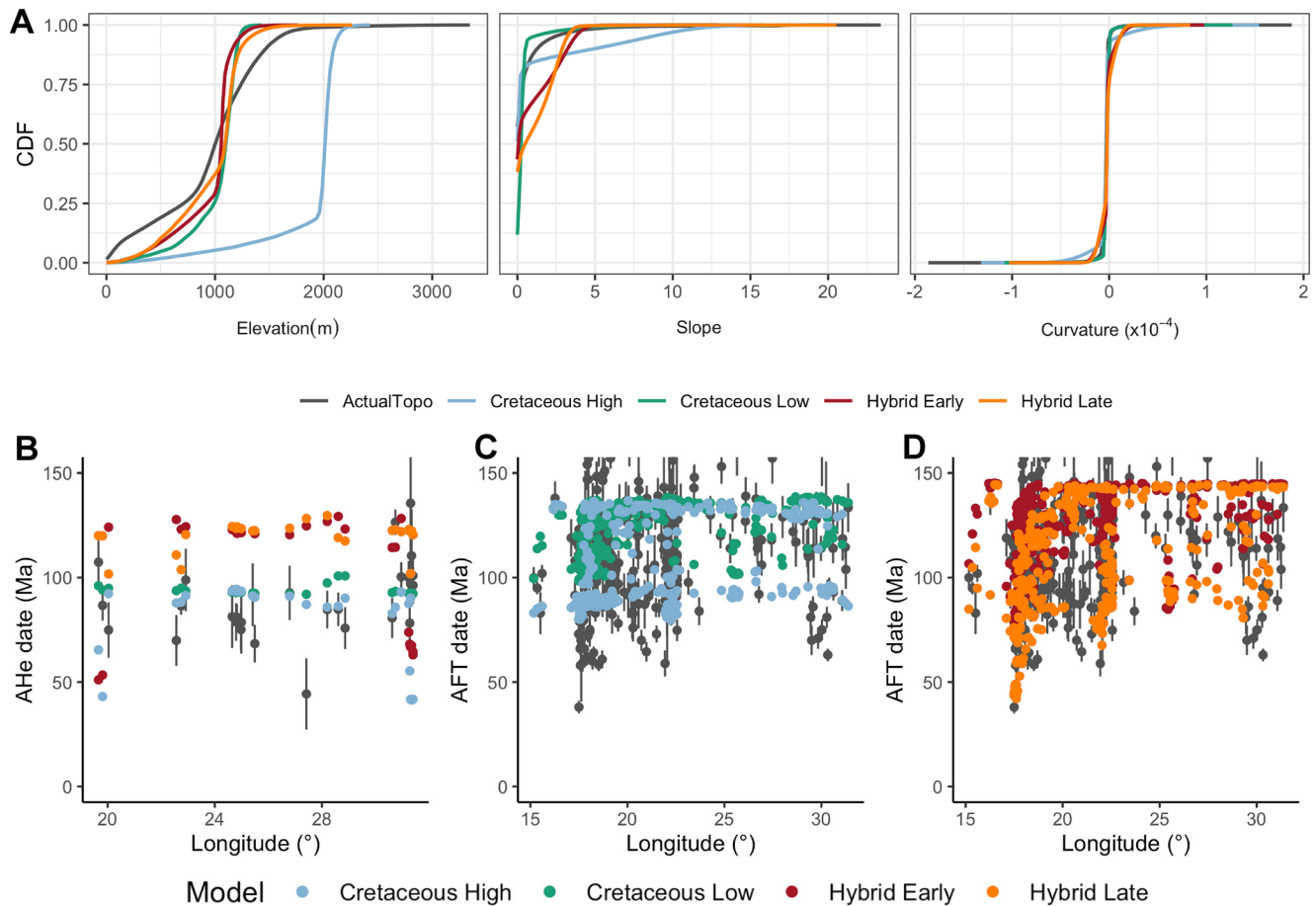


Figure 9. (a) Comparison of CDFs of present day southern African topographic metrics (gray) to best fit model runs from the Cretaceous High Scenario (blue), the Cretaceous Low Scenario (green), Hybrid Early Scenario (red) and Hybrid Late Scenario (orange). (b) AHe dates plotted by longitude for observed data (gray) and modeled dates from the best fit scenarios (colors as in a). (c) AFT dates plotted by longitude for observed data and two Cretaceous Scenarios. (d) As in (c) but the modeled data for the Hybrid Scenarios. Models split between (c) and (d) for better visibility.

the AFT data on the western margin (Figures 9c and 9d). When all data types are considered together, the models show similar fits to the total data set though the Cretaceous High scenario is somewhat worse on the elevation and sediment flux. While the three models do not reproduce all the details and structure in the natural data, they are a good match to the large-scale patterns observed (Figures 8 and 9).

5. Discussion

5.1. The Role of Data and the Misfit Function in Identifying Suitable Models

A major and initially surprising take-away from the inversion results is that the existing data cannot differentiate between these low misfit parameter sets, at least with the data we included and the current formulation of the misfit function. The uplift histories highlighted by the model inversions broadly match with times when plateau development had previously been proposed based on interpretation of the data sets that we have included (Table 1). We cannot settle the timing of uplift debate based on our results at present, but we can provide some insight into what is controlling the inversion results and what this means for erosion and uplift processes active in southern Africa.

The results of the model run are highly sensitive to the data used, the uncertainties associated, and the formulation of the misfit function. We constructed the misfit function to measure how well the model is able to capture the large-scale trends in the data that we see as most important: the major pulse of erosion and sedimentation observed in the Cretaceous, low sedimentation and erosion rates observed in the Cenozoic, and

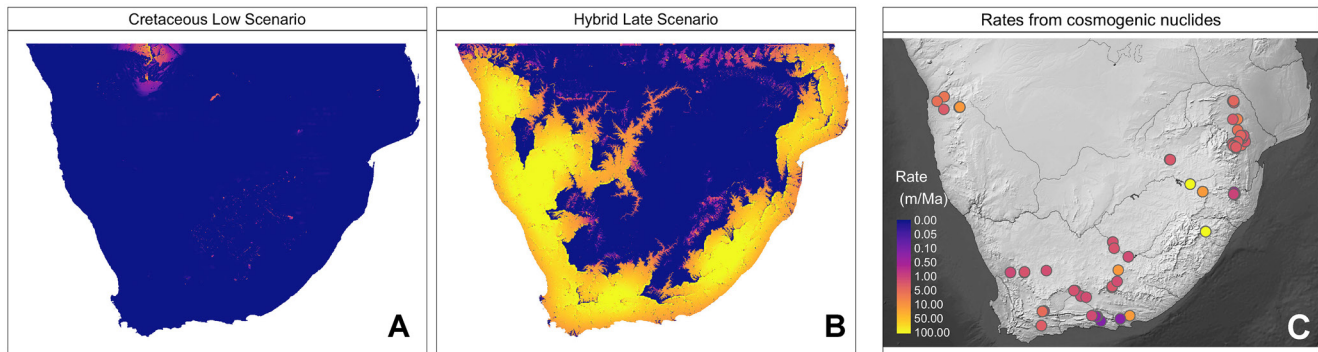


Figure 10. Predicted erosion rates for last 1 Myr timestep from the Cretaceous Low and Hybrid Late best fit models (a, b) compared with recent erosion rates (over the last 0.1–2 Myr) derived from cosmogenic radionuclide studies (c). Data in (c) are published data from bedrock samples or river incision rates at particular locations (Bierman et al., 2014; Cockburn et al., 2000; Decker et al., 2013; Dirks et al., 2016; Erlanger et al., 2012; Glotzbach et al., 2016; Keen-Zebert et al., 2016; Kounov et al., 2007, 2015; Scharf et al., 2013).

plateau-like topography with similar statistical characteristics to the current topography. We made choices in constructing a misfit function that reflect our view of these as important aspects of the data. However, different formulations of a misfit function are possible and would strongly affect the inversion results. For example, there many techniques have been utilized for comparing model outputs to topography (e.g., Barnhart et al., 2020; Howard & Tierney, 2012; Ibbitt et al., 1999; Skinner et al., 2018) that range from direct pixel comparisons which retain the spatial information to wholly aggregated statistical comparisons. We have chosen to compare statistical distributions using the KS statistic because this is an appropriate measure of the broad similarities between the topographies, but if the aim was to reproduce specific topographic features a different metric might be more appropriate and could change the inversion result.

The comparison of the modeled and observed thermochronology data is particularly nuanced because the prediction of the thermochronology data relies on the landscape model, the thermal model, and the kinetic model used to predict the data. We used kinetic models for Durango apatite (Crowley et al., 1991; Farley, 2000) to predict both the AFT and AHe dates. These models do not account for higher retentivities for fission tracks in Cl rich apatite (e.g., Green et al., 1986) and He in apatite with radiation damage (e.g., Shuster et al., 2006). Both these effects could cause higher closure temperatures in the samples. This may lead to an underprediction of the amount of material removed. Overall, kinetic differences could cause changes in the total magnitude of denudation between these phases, but we would not expect major differences in the relative magnitude between phases or between model scenarios.

Additionally, combining the metrics from different data types requires some challenging decisions about whether and how to weight the different data types. We have chosen not to weight the different misfits, and just sum them as the simplest solution. However, because the flux and thermochronology misfits take the form of least squares differences and can range from 0 to large values while the topographic misfits can only range from 0 to 1, the combined misfit is more sensitive to the thermochronology and flux misfits even though we do not directly weight them. For example, the Cretaceous Low Scenario fits the topography best (Figure 9a) so weighting the topography fit more heavily could reduce the misfits for models in that family of models relative to the other Scenarios. However, we feel that the weighting we used is appropriate and that our inversion yields model results that fit all data types adequately compared with the several other misfit formulations that we tested. Other choices about weighting of the different data types could be made, and these choices could substantially affect the inversion results.

Finally, the data included for comparison with model results strongly affects the inversion, and the inclusion of additional data has the potential to differentiate between these model scenarios. In fact, the results presented here can be used to guide future data collection efforts and highlight what additional information would be most useful in constraining the uplift histories of southern Africa. For example, the best fit models predict very different erosion rates in the final 1 Myr timestep (Figure 10), with the Hybrid Late Scenario predicting higher erosion rates focused along the main river network in canyons and near the coast while the Cretaceous Low Scenario predicts very low erosion rates throughout the landscape. Cosmogenic

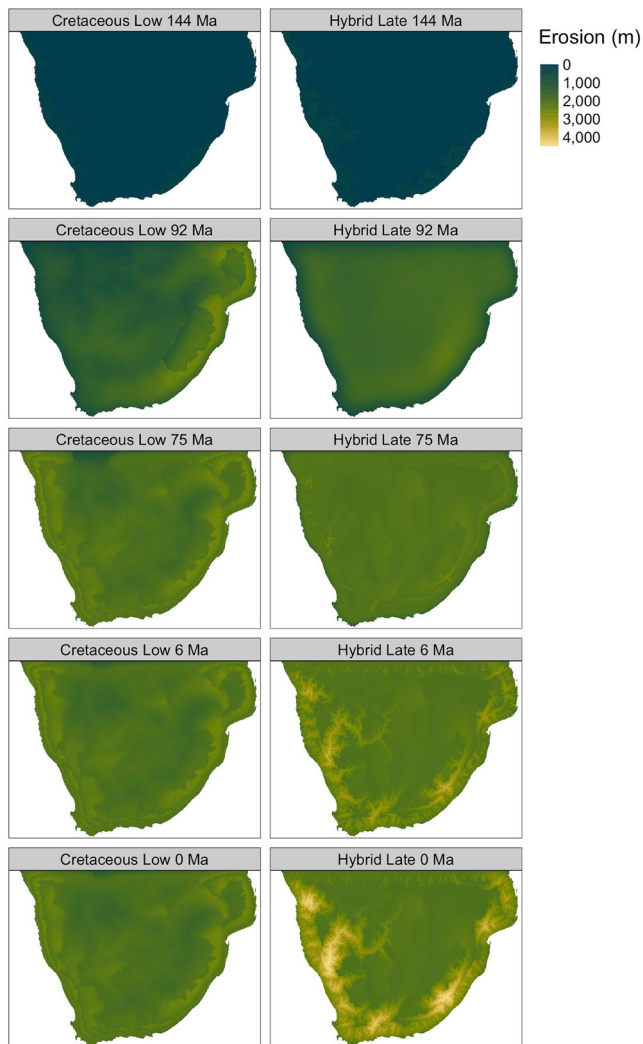


Figure 11. Erosion of the best fit models for the Cretaceous Low and Hybrid Late Scenarios throughout the model run. Highlights just after the start of the model (144 Ma), during tilting (92 Ma), after of tilting (75 Ma), and just after block uplift for the Hybrid Late Scenario (6 Ma) to the end (0 Ma).

radionuclide-based bedrock erosion rates could be compared to these predictions. Published cosmogenic radionuclide based erosion rates for southern Africa are mostly low (on the order of 1–10 m/Myr, Figure 10; Cockburn et al., 2000; Decker et al., 2013; Dirks et al., 2016; Erlanger et al., 2012; Fleming et al., 1999; Kounov et al., 2007; Makhubela et al., 2019; Scharf et al., 2013) but are generally not from within major river canyons, making it difficult to compare where the two landscape models differ the most prominently. One study focused directly on river valleys fairly high in the river systems near the drainage divide yields rates an order of magnitude higher (12–255 m/Myr), indicating there might be some spatial variation (Keen-Zebert et al., 2016). However, terraces in the lower Orange River suggest a maximum incision rate of 6 m/Ma post-17 Ma (M. C. J. de Wit, 1999), so we cannot fully distinguish between models based on published data.

5.2. Controls on Erosional Response to Uplift

One of the challenges in elucidating paleotopography is how to quantitatively link erosion rates or magnitudes derived from the rock record to changes in surface uplift or topography. We make the assertion that we expect an erosional response to topographic uplift, but the question is how much uplift is required to trigger erosion of a given magnitude, and what might cause that to vary. By comparing to both topographic and erosional metrics in our inversions, the results give us some insights into which parameters are most strongly controlling the magnitude of erosion in response to the uplift we impose in the model, and what that might mean for southern Africa's uplift history. We find that in this case, the ratio between the erosivity coefficient, K_f , and our parameterization of an erosion threshold, ϵ_c , plays an important role in the magnitude and temporal span of erosion after an uplift event. We also find that the shape of the uplift (tilting or block uplift) strongly affects the magnitude of erosion.

Braun et al. (2014) have already shown that continental tilting combined with a soft Karoo layer overlying harder basement was key for producing a sediment pulse similar to the major Cretaceous pulse in the Orange River Basin. Our results support that tilting is important and able to produce a large erosion response by steepening the slopes across the interior of the continent. Other shapes of uplift that we tried either disrupted the large, west draining Orange River drainage network, did not reproduce the sediment pulse, or both. In addition to the tilting, we found that adding

a parameter representing a threshold for erosion was critical for reproducing the pulse as well as the low sedimentation rates observed on the southern coast and throughout the Cenozoic. Without this threshold, models would continue to erode substantially, especially around the plateau margins even after the continent was no longer tilted. There is a clear covariation between the threshold parameter, ϵ_c , and the erosivity, K_f (Figure 5a), and parameter sets outside this band were not able to create the observed sediment pulse.

The Cretaceous uplift phase in all low misfit scenarios can produce similar magnitudes of erosion and sedimentation with very different magnitudes of uplift for different models (Figure 11). The parameters controlling the magnitude of erosion in response to a given uplift magnitude are K_f and its ratio to ϵ_c . The two Hybrid Scenarios values for K_f that differ by almost two orders of magnitude, but the ratio between K_f and ϵ_c is similar and they fall on the same trend when K_f and ϵ_c are plotted for these models (Figure 5a). This contrasts to the Cretaceous Low Scenario which has a higher ϵ_c for a given K_f (Figure 5a). The Cretaceous Scenario Low has higher magnitudes of Cretaceous uplift and tilting, ~1,300 m as compared to ~650 m in the Hybrid Scenarios, but a relatively higher threshold ($\epsilon_c/K_f = 126$). Higher magnitudes of uplift and

tilting are needed for stream power to exceed the threshold, but once exceeded, higher erosivity and steep slopes allow the model to erode relatively quickly. The Hybrid Scenarios, which only has ~650 m of uplift during Cretaceous tilting, has a lower erosivity, but also a lower threshold with $\varepsilon_c/K_f = 6$ and 25 for the best fit models, so less tilting is needed to exceed the threshold. The range in uplift magnitudes able to produce a similar erosion response highlights the difficulty in inferring uplift directly from erosion records, but also highlights the utility of landscape models, even fairly simple ones, to explore the range of possibilities. K_f and ε_c are generally not well known over large spatial and temporal scales, but this also highlights that if their values were well constrained they could differentiate between these uplift histories since each uplift scenario occupies distinct regions of parameter space for K_f and ε_c (Figure 5).

Changes in climate and precipitation will also affect the erosional response to uplift. We have kept K_f and precipitation constant throughout the model run, but evidence suggest southern Africa was more humid in the Late Cretaceous and became more arid in the Miocene (Braun et al., 2014; Pickford et al., 1999; Sandersen, 2007; Senut et al., 2009). We tested whether increasing rainfall alone could reproduce the major Cretaceous pulse of sediment, but found that an unreasonably high increase in rainfall was necessary (Figures S1 and S2). Thus, precipitation could have enhanced the erosional response to Cretaceous uplift and dampened the erosional response to Cenozoic uplift but cannot be driving erosion alone.

The low magnitude erosional response to widely varying Cenozoic uplift in the two families of models further highlights the importance of the shape and style of uplift for how much erosion occurs. One of the longstanding debates about southern African topography is how much of the topography is “recent” which we define here as Cenozoic. The debate centers on two groups of apparently contradictory observations: geometric and geomorphic evidence supporting recent uplift, and extremely limited post-Cretaceous sedimentation and erosion arguing against a major recent uplift event. Historically, most of the evidence for recent uplift was based on landforms that lacked quantitative dating (e.g., King, 1942; Partridge & Maud, 1987), though more recent work inverting river profile shapes also suggests recent uplift (Paul et al., 2014; Roberts & White, 2010; Rudge et al., 2015). Terraces on the lower Orange River suggest only 80–100 m of post-Miocene incision and upstream at the Vaal-Orange confluence only 120–140 m of incision (M. C. J. de Wit, 1999). Geometries of stratigraphic architecture indicate continental uplift on the order of a few hundred meters at ~25 Ma on the east coast (Baby, Guillocheau, Boulogne, et al., 2018; Baby, Guillocheau, Morin, et al., 2018), and Pliocene marine terraces have been uplifted to ~400 m above sea level near Gqeberha (Port Elizabeth) (McMillan, 1990). In contrast, magnitudes of erosion since the Cretaceous are negligible in some locations by the preservation of crater facies kimberlites (Scholtz, 1985; Smith, 1986), and limited to less than 1–4 km by extensive low-temperature thermochronology (Brown et al., 2002, 2014; Flowers & Schoene, 2010; Gallagher & Brown, 1999a; Kounov et al., 2009, 2013; Raab et al., 2005; Stanley et al., 2013, 2015; Stanley & Flowers, 2020; Tinker et al., 2008b; Wildman et al., 2015, 2016, 2017). Quantitative evidence on erosion has shown that erosion rates over the last ~2 Ma were slow based on cosmogenic nuclides (Bierman et al., 2014; Chadwick et al., 2013; Decker et al., 2013; Dirks et al., 2016; Fleming et al., 1999; Kounov et al., 2007). There is very limited offshore sedimentation in the Cenozoic, also suggesting low erosion magnitudes on the continents (Baby, Guillocheau, Boulogne, et al., 2018; Baby et al., 2020; Baby, Guillocheau, Morin, et al., 2018; Guillocheau et al., 2012; Rouby et al., 2009; Tinker et al., 2008a), and near Cape Town, essentially no incision since the Miocene (Roberts et al., 2013). Together this suggests either limited recent surface uplift or that almost no erosion was caused by any recent uplift.

One way to reconcile these seemingly contrasting observations (geometric evidence for recent uplift but very low erosion rates) is if surface uplift does not trigger a large erosional response. The Hybrid Scenario models demonstrates that limited erosion in response to substantial surface uplift is possible from a geomorphic standpoint. Normally, surface uplift is thought to trigger an erosional response by steepening slopes and increasing stream power and therefore erosion rates. In the case of the Hybrid Scenarios, block uplift of an already low-relief plateau only causes steepening in very focused locations in river channels. Therefore, even though substantial topography is developed in the Cenozoic in the Hybrid Scenario, the erosional response is subdued across most of the landscape, reconciling the low eroded volumes and generally low erosion rates with geometric evidence for surface uplift.

5.3. Source-to-Sink Mass Balance

The interest in topographic evolution, confined marine basins, and limited to absent continental sediment storage in southern Africa make it an advantageous location to study source-to-sink relationships. The extensive data coverage and the use of the landscape model to directly calculate denudation magnitudes and thermochronology dates with an evolving crustal thermal structure allows us to examine the source-to-sink mass balance more holistically than previously possible. Past work compared estimated onshore denudation through time from AFT data to marine sediment volumes on the west coast and the south coast with differing results. Rouby et al. (2009) compared the marine sediment volumes from the west coast basins to AFT derived denudation magnitudes for the western margin of southern Africa and Namibia (Gallagher & Brown, 1999a, 1999b) and found a reasonably good match of the volumes through time with the exception of the Cenozoic. On the southern margin, Tinker et al. (2008a, 2008b) compared the AFT derived denudation and sediment volume in the Outeniqua Basin and found that the marine sediment volumes were an order of magnitude less than onshore denudation volumes, though the timing of denudation and deposition match well (Tinker et al., 2008a). The marine sediment volumes calculated by Tinker et al. (2008a) were based on only the shelf volumes, so any material deposited in the deep sea was unaccounted for (Baby et al., 2020; Tinker et al., 2008a). Richardson et al. (2017) estimated the eroded volume on the south coast using geometric reconstruction of onshore sedimentary units and suggested that only one third to one half of the eroded volume was contained in the Outeniqua Basin.

Our model provides a new way to examine this question by searching for erosion histories that can match both the thermochronology data and the offshore sediment volumes. There are several key parameters used to calculate thermochronology dates from erosion histories, and by examining the ranges of these parameters that can satisfy both the thermochronology and the sediment data we can gain insights into source-to-sink relationships. Thermochronology is highly sensitive to the upper crustal thermal structure, and previous thermochronology based denudation estimates (Gallagher & Brown, 1999a, 1999b; Tinker et al., 2008b; Wildman et al., 2015, 2016) made some set of assumptions for this structure through time, which could be a source of uncertainty when comparing onshore denudation and offshore volumes. We calculate the thermal structure throughout the model run, and key parameters controlling the structure are the temperature at the base of the model (T_{\max}), the ratio between the thermal diffusivity of the basement and the overlying Karoo sedimentary rocks (R_K). We vary both T_{\max} and R_K , as well as adding an additional non-thermal parameter which represents the ratio of sediment volume lost between onshore erosion and offshore deposition (R_D). Surface geothermal gradients for our best fit models range from 38 to 46°C/km, fairly high geothermal gradients resulting from high temperatures at the base of the model and significant thermal blanketing by the Karoo Supergroup (Tables 2 and 3). Average geothermal gradient for southern Africa are estimated to be 15–33°C/km on average (Macgregor, 2020) though heat flow varies widely with high heat flow in mobile belts thought to be due to higher heat flow in thinner lithosphere (e.g., Jones, 1987; 2017). The higher geothermal gradients in the upper crust of our models requires lower magnitudes of exhumation to produce the observed thermochronology dates. Even with these values for the thermal parameters, low misfit models converge on values of the deposition ration, R_D , where only 1/2 to 1/4 of the eroded material is deposited in the basins (Figure 4k).

There are several caveats to this ratio, however. The first is that there are tradeoffs between all of these parameters. More extreme geothermal gradients or thermal diffusivity ratios (outside the range over which parameters were allowed to vary) would require less denudation to satisfy the thermochronology data, yielding a lower mismatch between the predicted and observed volumes. Additionally, while the predicted sediment volumes match the observed sediment volumes well for certain times throughout the model run, particularly in the Cretaceous, there are other times when the model predictions underestimate the volume of sediment (Figure 7). Since at times the model underestimates the sediment volume, the ratio of sediment loss implied by the parameter R_D in the low misfit models is likely an upper limit for sediment loss. Also, in reality the ratio of sediment loss may have been variable through time while R_D is fixed throughout a model run. Despite these caveats, the models suggest that more material is eroded than deposited in the marine basins, perhaps greater than twice as much.

This, of course, begs the question of what happened to this “missing” sediment? We see three possible explanations: (a) material was removed from the system via tectonic transport out of the region, (b) material

was removed from the system via oceanic or eolian transport out of the area, or (c) material was removed from the continent via chemical denudation and therefore not deposited as a solid load in the basins. We favor substantial chemical denudation on the continent, but we will examine the evidence for each of these mechanisms.

There is clear evidence that some material eroded off the southern coast during the early portion of Gondwana breakup was deposited in the marine basins that are presently near the Falkland Plateau, now situated in the SW Atlantic Ocean. In the Late Jurassic and Early Cretaceous this basin was situated adjacent to the Outeniqua Basin (Baby, Guillocheau, Boulogne, et al., 2018; Dingle & Scrutton, 1974; Macdonald et al., 2003; Martin et al., 1982; Richardson et al., 2017; Williams, 2015). The North Falkland Basin contains continental facies, likely derived from southern Africa (Baby, Guillocheau, Boulogne, et al., 2018; Richardson et al., 2017; Williams, 2015). The main period of southern African deposition into this basin was ~135–130 Ma, after which transform motion on the Agulhas-Falkland Fracture Zone and eventual opening of the South Atlantic removed the North Falkland Basin from proximity to southern Africa (Baby, Guillocheau, Boulogne, et al., 2018; Dingle & Scrutton, 1974; Martin et al., 1982). Thus any sediment loss due to tectonic transport is limited to the Early Cretaceous.

Several erosional features and contourite deposits present on all margins show that sediments have been eroded and redistributed since the Early Cretaceous by oceanic processes and in some locations by winds (e.g., Baby, Guillocheau, Boulogne, et al., 2018; Garzanti et al., 2015; Hopkins, 2006; Thiéblemont et al., 2020; Uenzelmann-Neben et al., 2007). Oceanic current structures have been characterized at various depth since Aptian-Albian times (120–110 Ma) in Walvis and Zambezi Basins, but their role became major during Early Miocene (23–16 Ma, Hopkins, 2006; Thiéblemont et al., 2020; Uenzelmann-Neben et al., 2007). The ability of these oceanic currents to transport large volumes of sediment (in this case during Neogene time) is difficult to quantify, even though it is of primary importance in modeling source-to-sink systems. Concerning surficial currents, Orange River sand is known to be transported 1,000+ km northward up the Namibian coast via littoral drift (e.g., Garzanti et al., 2018) but the amount of sand transported is estimated at 1,500–15,000 km³ over the last 15 Myr (Garzanti et al., 2018) which only amounts to a small fraction of the west coast sediment budget. Onshore, aeolian processes could be responsible for redistributing sediment. The climate today is arid to semi-arid. Miocene to recent dune deposits are found along the coast of Namibia with sand sourced from the Orange River (e.g., Garzanti et al., 2015; Ward, 1988), though the volume of transport is of unknown. However, from ~85 Ma to 15 Ma paleoprecipitation records suggest humid conditions in southern Africa (Bamford & Stevenson, 2002; Braun et al., 2014; Sandersen, 2007) making substantial aeolian transport during that period unlikely. Prior to ~85 Ma the Atlantic continental margin was more arid leaving wind transport a possibility, though deposits just offshore show fluvial channels and marshes not extreme aridity (Stevenson & McMillan, 2004). In summary, the magnitude of sediment lost due to oceanic and aeolian transport is unknown. It may be significant, particularly in the Miocene, but sediment lost this way varies in space and time.

Finally, chemical weathering on the continent could have been substantial. Basalts are particularly susceptible to chemical weathering (e.g., Dessert et al., 2003; Dupré et al., 2003) and much of the eroded material in the Cretaceous was Karoo flood basalts (e.g., Hanson et al., 2009; Stanley et al., 2015; Tinker et al., 2008a). The sedimentary rocks in the Karoo Supergroup are dominantly siliciclastic so have a lower chemical weathering potential than basalt but also could weather chemically under favorable conditions with sufficient time. Cretaceous erosion took place under climatic conditions much warmer than today, which could have promoted chemical weathering (e.g., Cohen et al., 2004; Jenkyns et al., 2004). A rough compilation of precipitation records based on paleobotanical data suggests a sharp change around 85 Ma from semi-arid to very humid conditions on both the Atlantic and Indian margins favoring intense silica weathering up to 40 Ma (Braun et al., 2014; Ponte et al., 2019; Sandersen, 2007). Deep weathering surfaces are found throughout southern Africa (e.g., Summerfield, 1983) and were forming throughout Africa from the Late Cretaceous through the Neogene (Guillocheau et al., 2018). Onset of weathering in weathering surfaces in north-central South Africa (Kuruman Hills) was dated at 77 ± 7.5 Ma (Vafeas et al., 2018). This is consistent with dating of weathering surfaces north of our study area in southern Congo (Katanga) where supergene manganese ore formed between 77 and 2 Ma with several peaks, demonstrating many phases of weathering and surface formation since the Cretaceous (De Putter & Ruffet, 2020). Within our study

area there is evidence for the role of chemical weathering in the denudation history in some locations (e.g., Chadwick et al., 2013; Margirier et al., 2019). Onshore chemical denudation during the Cretaceous in particular is supported by the offshore record where Late Cretaceous deltaic deposits are dominated by clays (Baby, Guillocheau, Morin, et al., 2018; Holtar & Forsberg, 2000; Paton et al., 2008), though detailed compositions and chemistries of these clays are not known.

Overall, our model results suggest that a substantial volume of material eroded from the continent was not accounted for in the sediment volumes presently in the marine basins. This sediment loss was likely due to a combination of factors, and the most important process may have varied through time. During the Early Cretaceous, sediment could have been deposited on the Falkland Plateau (e.g., Baby, Guillocheau, Boulogne, et al., 2018; Dingle & Scrutton, 1974; Martin et al., 1982), whereas oceanic currents and winds may have redistributed substantial volumes especially during the Neogene (e.g., Garzanti et al., 2015; Thiéblemont et al., 2020; Uenzelmann-Neben et al., 2007). Throughout the history, but especially during the Late Cretaceous and Paleogene, substantial denudation may have occurred via chemical processes resulting in less sediment deposited as a solid load in the basins. Our best fitting models match the observed sediment volumes best in the Late Cretaceous (Figure 8) with only $\sim 1/3$ of the eroded sediment being deposited in the basin. Climatic conditions were favorable for chemical weathering at that time (e.g., Braun et al., 2014) and we take our results to provide additional support that continental chemical weathering was an important process in southern Africa, especially in the Late Cretaceous and Paleogene.

5.4. Distinguishing Geodynamic Mechanisms for Plateau Uplift

Both the Cretaceous Scenarios and the Hybrid Scenarios predict some topographic development in the Cretaceous but the two scenarios differ in magnitude and the duration of continental tilting during this uplift phase. We can compare the rates and magnitudes from our models to those which might be expected from different geodynamic mechanisms for uplift. Because the Cretaceous High Scenario produces models that do not match present day topography, we consider it unlikely and focus on the Cretaceous Low Scenario and Hybrid Scenarios. These models all predict a total of $\sim 1,400$ m of dynamic topography by the end of the model run. This is within, but on the upper end, of the range of predicted magnitudes of present day dynamic topography in southern Africa, though it should be noted that these predictions vary widely (e.g., Flament et al., 2013). However, the Cretaceous and Hybrid scenarios differ in the timing and rate of topographic development (Figure 12). The Cretaceous Scenario has a much higher uplift magnitude during dynamic tilting than the Hybrid scenarios ($\sim 1,300$ m vs. ~ 650 m for their respective best fit models, Figure 12). We can also compare both vertical uplift rates and horizontal propagation rates. One of the fixed parameters in all models is that the dynamic uplift occurs linearly over 5 Myr. The Cretaceous Scenario then has a dynamic uplift rate of 0.26 mm/yr, while the Hybrid Scenario uplifts at a rate of 0.13 mm/yr. To approximate the horizontal propagation rates for the uplift signal, we can use the tilt time parameter and the width of the model. The tilt time parameter is the time delay between the east side of the model initiating uplift and the west side (Figure 12). In essence, it is the amount of time taken for the uplift to propagate across the model domain. A rough estimate of the horizontal propagation rate that can be compared to plausible geodynamic deformation rates is given by dividing the 2,365 km wide model domain by the tilt time (6.1 Myr for the best fit Cretaceous Low Scenario and 11.6 Myr for the best fit Hybrid Late Scenario, though tilt times for Hybrid models range widely). The propagation rate of the uplift is then 39 cm/yr for the Cretaceous Scenario and 21 cm/yr in the Hybrid Late Scenario.

Braun et al. (2014) proposed that tilting and dynamic uplift of the plateau was caused by movement of the African plate over the LLSVP in the deep mantle. In this conceptual model, rates of horizontal propagation should be set by plate motion rates. Both the Cretaceous and Cenozoic propagation rates are fast for plate motion rates, but the Cretaceous Scenario especially so. Plate motion rates reconstructed for Africa in the mid-Cretaceous vary. Colli et al. (2014) reconstructed absolute plate speeds for a point in the northwest quadrant of our model (27°S , 15°E) using the Müller et al. (1993) fixed hotspot reference frame and a combination of the O'Neill et al. (2005) and Steinberger and Torsvik (2008) moving hotspot and true polar wander models. The fixed hotspot frame gave velocities increasing from <1 to ~ 3 cm/yr from 110 to 90 Ma (Colli et al., 2014; Müller et al., 1993), while the moving hotspot and true polar wander models gave velocities ranging from ~ 2 to 4 cm/yr between 110 and 90 Ma with a major spike to >10 cm/yr between 105 and

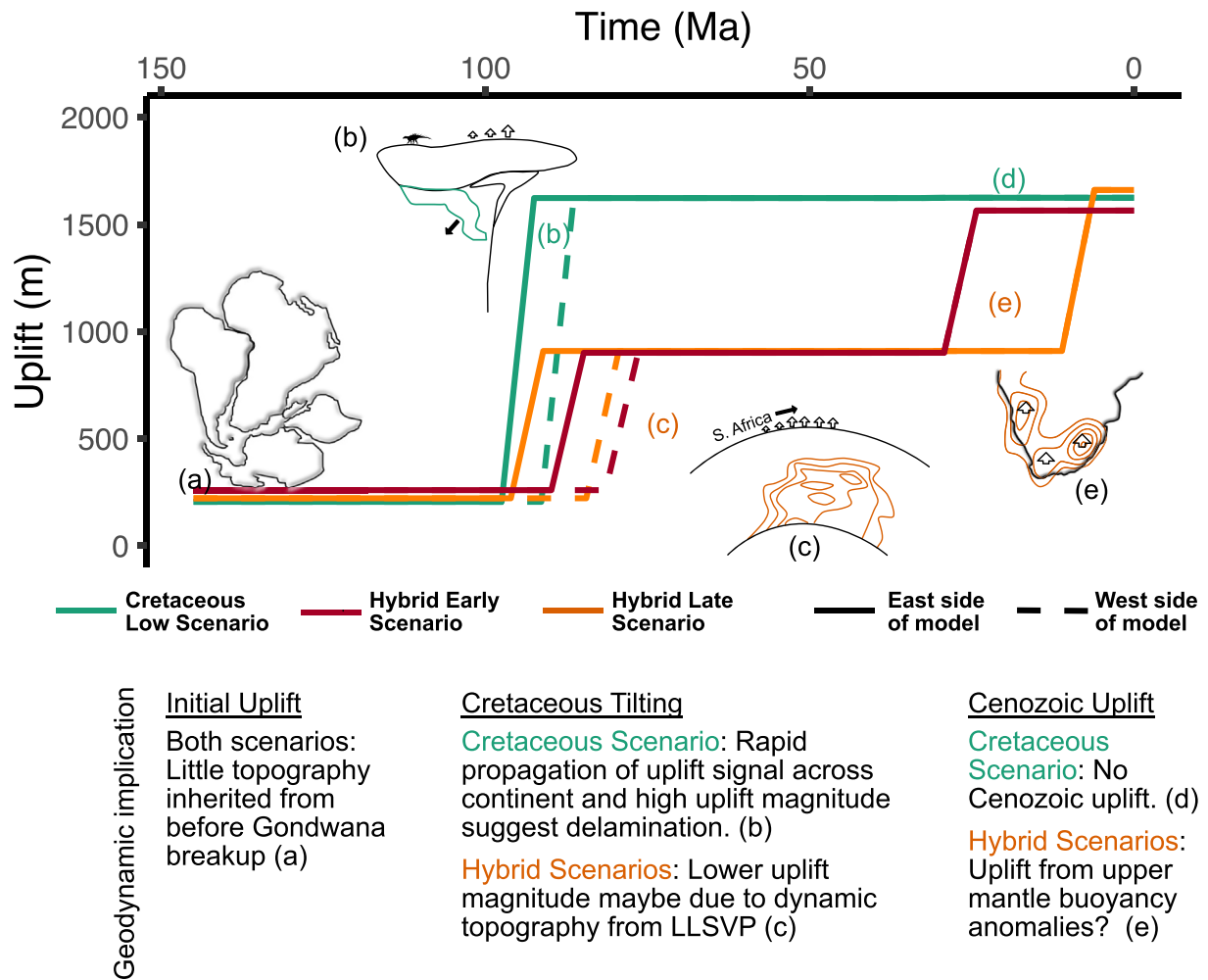


Figure 12. Geodynamic implications of the model results. Lines on graph show uplift over time for best fit models from the low misfit regions of model results. Cartoons show the implied geodynamic mechanism for each uplift phase. See text for a more complete discussion and Table 1 for more on geodynamic hypotheses.

100 Ma (Colli et al., 2014; O'Neill et al., 2005; Steinberger & Torsvik, 2008). These rates are all substantially below the ~ 40 cm/yr predicted by the Cretaceous Scenario but get a little closer to the ~ 20 cm/yr predicted by the Hybrid Scenario at times.

In addition to propagation rates that are too fast to be dictated by plate motion of southern Africa riding over the LLSVP, the Cretaceous Scenario requires a high magnitude of Cretaceous topography, $\sim 1,400$ m. While initial work suggested that this magnitude of dynamic topography could be attributed to the LLSVP (e.g., Lithgow-Bertelloni & Silver, 1998), more recent studies suggest that the large degree-two lower mantle structures have a more limited influence on dynamic topography at the surface (Hoggard et al., 2016; Osei Tutu et al., 2018; Steinberger, 2016; Steinberger et al., 2019; Watkins & Conrad, 2018). Together, this implies that if the Cretaceous Scenario is the correct model, some other mechanism beyond dynamic topography over the LLSVP needs to be invoked to explain the rapidity and magnitude of elevation gain. Removal of mantle lithosphere either through delamination or dripping of convective instabilities could potentially generate these magnitudes and rates. Hu et al. (2018) proposed a delamination-style peeling back of the lowermost lithosphere triggered by motion over hotspots, also implying that rates would dominantly be controlled by plate motion rates. However, at least for lithospheric drips, dynamic models show that once instabilities form, they can grow exponentially or even super exponentially depending on the wavelength of the perturbation and the viscosity structure (e.g., Conrad & Molnar, 1997; Molnar et al., 1998). So perhaps once destabilized the dense lower lithosphere could have been removed fairly rapidly. Dripping or

delamination can also produce surface uplift on the order of 1–2 km (e.g., Göğüş & Pysklywec, 2008a, 2008b) in line with the uplift required by Cretaceous Scenario. There is also evidence for Cretaceous lithospheric perturbation in southern Africa from elevated geothermal gradients recorded by mantle and lower crustal xenoliths (Bell et al., 2003; Schmitz & Bowring, 2003) and the coincidence of a major erosion phase with this warming geotherm (Stanley et al., 2013). If the Cretaceous Scenario is correct, we suggest much of the uplift of southern Africa was driven by lithospheric foundering rather than solely sublithospheric dynamic topography (Figure 12).

The Hybrid Scenarios have smaller magnitudes (400–800 m) of dynamic topography in the Cretaceous, followed by ~800 m of uplift in the Cenozoic. Retrodictions of dynamic topography back through the Cretaceous are somewhat limited, but several predict the development of 200–500 m of dynamic topography during the early Late Cretaceous, due to motion over the LLSVP and/or motion away from the South American subduction zone (Flament et al., 2014; Rubey et al., 2017; Zhang et al., 2012). Motion of southern Africa over the LLSVP and deep-mantle derived dynamic topography seems to provide a suitable explanation for the magnitudes and rates of Cretaceous topographic development in the Hybrid Scenario (Figure 12). Interestingly, the peak in southern African plate motion rate in the moving hotspot/true polar wander reference frame (Colli et al., 2014; O'Neill et al., 2005; Steinberger & Torsvik, 2008) most closely corresponds with the rates in the Hybrid Scenarios and also coincides with the initiation of Cretaceous uplift. Colli et al. (2014) argued that changes in South Atlantic spreading velocities are related to topographic changes on the continents through pressure driven flow in the asthenosphere. Together this highlights the links between the deep earth, plate motions, and continental erosion. An additional ~800 m of Cenozoic dynamic topography in the Hybrid Scenarios onsets at 40–10 Ma depending on the model. The onset of uplift in the Early Hybrid scenario also coincides with a rapid phase of south Atlantic spreading at ~35–30 Ma (Colli et al., 2014), as well as the proposed timing for development of small-scale convection beneath Africa (Burke, 1996), and overlaps with development of the East Africa Rift system (e.g., Ebinger & Sleep, 1998; Roberts et al., 2012). Development of this Cenozoic topography seems more likely to be derived from upper mantle density anomalies than the LLSVP, though both could contribute (Hoggard et al., 2016; Winterbourne et al., 2009).

The Hybrid and Cretaceous Scenarios have different magnitudes and rates of uplift, implying different driving mechanisms for uplift (Figure 12). The Cretaceous Scenario is more consistent with uplift driven by destabilization and delamination of the lithosphere whereas the Hybrid Scenario is more consistent with uplift driven by motion over the LLSVP and upper mantle dynamic topography.

6. Conclusions

We used inversion methods to compare landscape models varying a range of uplift, erosion, and thermal parameters with observed offshore sediment volumes, thermochronology data, and topography from Southern Africa. We explored three proposed hypotheses for when the plateau was elevated and found good matches to four possible uplift histories (Figure 3). Two suitable models have plateau development entirely in the Cretaceous, with ~1,400 m or >2,300 m of dynamic uplift and continental tilting initiating between 100 and 90 Ma. Because the model scenario with high magnitudes of Cretaceous tilting does not match the present day topography, we do not favor it as a likely uplift history. The other two families of suitable models have two phase plateau development with ~400–800 m of dynamic uplift and continental tilting initiating at ~100–90 Ma followed by ~500–1,000 m of dynamic block uplift either at ~40–20 Ma or at 10 Ma (Figure 6). The data that we used cannot distinguish between these two uplift histories, though stratigraphic architecture at the margins suggests two phases of uplift (Baby, Guillocheau, Boulogne, et al., 2018; Baby et al., 2020; Baby, Guillocheau, Morin, et al., 2018). However, model predictions can be used to identify data that could be used to differentiate between these models.

Results from these models give some insight into the link between erosion rate, uplift, and topography in southern Africa. Good fitting models show an important relationship between the uplift history and the magnitudes of the erosivity constant, K_f , and our parameterization of an erosion threshold, ϵ_c (Figure 5). This suggests that a fairly high threshold is important for maintaining uplifted topography over long periods of geologic time with low erosion and sedimentation rates. In addition to the erosive parameters, the erosional response to uplift is highly sensitive to the shape of the uplift. Our models show that continental

scale tilting can cause a high magnitude erosional response for a range of uplift amounts due to steepening of the entire drainage network and stability or enhancement of large drainages. This is in line with previous work (Braun et al., 2013, 2014) and is important for reproducing the pulsed nature of Cretaceous erosion and sedimentation in southern Africa. In contrast, the block uplift shape produces a relatively small erosional response for significant magnitudes of uplift because much of the plateau interior does not steepen (Figure 11). These conditions are able to reconcile geometric evidence for Cenozoic uplift with the observed low magnitudes of erosion.

Source-to-sink mass balance between the amount of material eroded implied by the thermochronology data and the amount deposited in the offshore basins suggests a substantial amount of mass loss. Best-fit models suggest about 3 times as much material was eroded as deposited, though this is likely an upper bound. While some material could have been transported away by ocean currents, wind, or tectonics (e.g., Garzanti et al., 2018; Richardson et al., 2017), we argue that this is supporting evidence for chemical denudation, where a portion of the material removed from the continent was transported in solution to the ocean and therefore not directly deposited in marine basins.

Finally, while the data cannot distinguish between the Cretaceous and Hybrid best fit models at the present, the relative rates of deformation and magnitudes of surface change might help discriminate between the geodynamic mechanisms which could be driving them (Figure 12). For the Cretaceous Scenario, the propagation of the uplift signal during continental tilting is likely too rapid to be only related to plate tectonic motion, and uplift magnitudes are higher than expected for dynamic uplift due to the LLSVP. Uplift in this case may be more likely to be driven by processes that can act faster and cause more surface change like delamination (e.g., Göğüş & Pysklywec, 2008b; Hu et al., 2018) than by the African Plate moving over the LLSVP (Braun et al., 2014). However, in the Hybrid Scenarios uplift magnitudes are lower and potentially propagate more slowly across the continent. Thus, tilting as the African Plate rides over the LLSVP is a plausible uplift mechanism.

Data Availability Statement

All data included in the modeling have been previously published and is available in Amante and Eakins (2009), Baby et al. (2020), Belton and Raab (2010), Brown (1992), Brown et al. (1990, 2002, 2014), M. C. J. De Wit (1988), Flowers and Schoene (2010), Green et al. (2017), Kounov et al. (2009, 2013), Raab (2001), Raab et al. (2002), Stanley et al. (2013, 2015), Stanley and Flowers (2020), Tinker et al. (2008b), and Wildman et al. (2015, 2016, 2017). Data are summarized with publication information specified for individual data points in the supplemental materials. The code used to generate all model results is archived with Zenodo (Braun & Stanley, 2020) as is all of the input data, configuration, and results (Stanley, 2020).

References

- Al-Hajri, Y., White, N., & Fishwick, S. (2009). Scales of transient convective support beneath Africa. *Geology*, 37(10), 883–886. <https://doi.org/10.1130/g25703a.1>
- Amante, C., & Eakins, B. W. (2009). *ETOPO1 arc-minute global relief model: Procedures, data sources and analysis*.
- Baby, G. (2017). *Mouvements verticaux des marges passives d'Afrique australe depuis 130 Ma, étude couplée: Stratigraphie de bassin: Analyse des formes du relief* (PhD thesis, p. 363). Université de Rennes 1.
- Baby, G., Guillocheau, F., Boulogne, C., Robin, C., & Dall'Asta, M. (2018). Uplift history of a transform continental margin revealed by the stratigraphic record: The case of the Agulhas transform margin along the Southern African Plateau. *Tectonophysics*, 731–732, 104–130. <https://doi.org/10.1016/j.tecto.2018.03.014>
- Baby, G., Guillocheau, F., Braun, J., Robin, C., & Dall'Asta, M. (2020). Solid sedimentation rates history of the Southern African continental margins: Implications for the uplift history of the South African Plateau. *Terra Nova*, 32(1), 53–65. <https://doi.org/10.1111/ter.12435>
- Baby, G., Guillocheau, F., Morin, J., Ressouche, J., Robin, C., Broucke, O., & Dall'Asta, M. (2018). Post-rift stratigraphic evolution of the Atlantic margin of Namibia and South Africa: Implications for the vertical movements of the margin and the uplift history of the South African Plateau. *Marine and Petroleum Geology*, 97, 169–191. <https://doi.org/10.1016/j.marpetgeo.2018.06.030>
- Bamford, M. K., & Stevenson, I. R. (2002). A submerged Late Cretaceous podocarpaceous forest, west coast, South Africa : Research letter. *South African Journal of Science*, 98(3–4), 181–185.
- Barnhart, K. R., Tucker, G. E., Doty, S., Shobe, C. M., Glade, R. C., Rossi, M. W., & Hill, M. C. (2020). Inverting topography for landscape evolution model process representation: Part 2, calibration and validation. *Journal of Geophysical Research: Earth Surface*, 125(7), e2018JF004963. <https://doi.org/10.1029/2018JF004963>
- Bell, D. R., Schmitz, M. D., & Janney, P. E. (2003). Mesozoic thermal evolution of the southern African mantle lithosphere. *Lithos*, 71(2–4), 273–287. [https://doi.org/10.1016/s0024-4937\(03\)00117-8](https://doi.org/10.1016/s0024-4937(03)00117-8)

Acknowledgments

Support for this project was provided by the Alexander von Humboldt Foundation. We thank Lukas Becker for reading an early version of the manuscript and members of the Earth Surface Processes Modeling group at the GFZ for helpful feedback and discussions. Thoughtful reviews by M. G. Fellin, G. Jepson, and Associate Editor P. DeCelles are much appreciated and helped improve the manuscript. Many figures were made using the R packages ggplot2 (Wickham, 2016), tmap (Tennekes, 2018), and rayshader (Morgan-Wall, 2020).

Open access funding enabled and organized by Projekt DEAL.

- Belton, D. X., & Raab, M. J. (2010). Cretaceous reactivation and intensified erosion in the Archean–Proterozoic Limpopo Belt, demonstrated by apatite fission track thermochronology. *Tectonophysics*, *480*(1–4), 99–108. <https://doi.org/10.1016/j.tecto.2009.09.018>
- Bierman, P. R., Coppersmith, R., Hanson, K., Neveling, J., Portenga, E. W., & Rood, D. H. (2014). A cosmogenic view of erosion, relief generation, and the age of faulting in southern Africa. *Geological Society of America Today*, *24*(9), 4–11. <https://doi.org/10.1130/gsatg206a.1>
- Bluck, B. J., Ward, J. D., & De Wit, M. C. J. (2005). Diamond mega-placers: Southern Africa and the Kaapvaal craton in a global context. *Geological Society, London, Special Publications*, *248*(1), 213–245. <https://doi.org/10.1144/gsl.sp.2005.248.01.12>
- Braun, J. (2002). Quantifying the effect of recent relief changes on age–elevation relationships. *Earth and Planetary Science Letters*, *200*(3), 331–343. [https://doi.org/10.1016/S0012-821X\(02\)00638-6](https://doi.org/10.1016/S0012-821X(02)00638-6)
- Braun, J. (2018). A review of numerical modeling studies of passive margin escarpments leading to a new analytical expression for the rate of escarpment migration velocity. *Gondwana Research*, *53*, 209–224. <https://doi.org/10.1016/j.gr.2017.04.012>
- Braun, J., Guillocheau, F., Robin, C., Baby, G., & Jelsma, H. (2014). Rapid erosion of the Southern African Plateau as it climbs over a mantle superswell. *Journal of Geophysical Research: Solid Earth*, *119*(7), 6093–6112. <https://doi.org/10.1002/2014jb010998>
- Braun, J., Robert, X., & Simon-Labric, T. (2013). Eroding dynamic topography. *Geophysical Research Letters*, *40*(8), 1494–1499. <https://doi.org/10.1002/grl.50310>
- Braun, J., & Stanley, J. R. (2020). FastScape landscape evolution model, Fortran version utilized for southern African model inversions. *Zenodo*. <https://doi.org/10.5281/zenodo.4150333>
- Braun, J., Van Der Beek, P., & Batt, G. (2006). *Quantitative thermochronology: Numerical methods for the interpretation of thermochronological data*. Cambridge University Press.
- Braun, J., & Willett, S. D. (2013). A very efficient O(n), implicit and parallel method to solve the stream power equation governing fluvial incision and landscape evolution. *Geomorphology*, *180*, 170–179. <https://doi.org/10.1016/j.geomorph.2012.10.008>
- Brown, R. W. (1992). *A fission track thermochronology study of the tectonic and geomorphic development of the sub-aerial continental margins of southern Africa (PhD)*. La Trobe University.
- Brown, R. W., Rust, D. J., Summerfield, M. A., Gleadow, A. J., & De Wit, M. C. (1990). An Early Cretaceous phase of accelerated erosion on the south-western margin of Africa: Evidence from apatite fission track analysis and the offshore sedimentary record. *International Journal of Radiation Applications and Instrumentation - Part D: Nuclear Tracks and Radiation Measurements*, *17*(3), 339–350. [https://doi.org/10.1016/1359-0189\(90\)90056-4](https://doi.org/10.1016/1359-0189(90)90056-4)
- Brown, R. W., Summerfield, M., Gleadow, A., Gallagher, K., Carter, A., Beucher, R., & Wildman, M. (2014). Intracontinental deformation in southern Africa during the Late Cretaceous. *Journal of African Earth Sciences*, *100*, 20–41. <https://doi.org/10.1016/j.jafrearsci.2014.05.014>
- Brown, R. W., Summerfield, M. A., & Gleadow, A. J. W. (2002). Denudational history along a transect across the Drakensberg Escarpment of southern Africa derived from apatite fission track thermochronology: Denudational history of the Drakensberg escarpment. *Journal of Geophysical Research*, *107*(B12). <https://doi.org/10.1029/2001jb000745>
- Burke, K. (1996). The African plate. *South African Journal of Geology*, *99*(4), 341–409.
- Burke, K., & Gunnell, Y. (2008). *The African erosion surface: A continental-scale synthesis of geomorphology, tectonics, and environmental change over the past 180 million years* (Vol. 201). Geological Society of America.
- Burke, K., & Wilson, J. T. (1972). Is the African plate stationary? *Nature*, *239*(5372), 387–389. <https://doi.org/10.1038/239387b0>
- Catuneanu, O., Wopfner, H., Eriksson, P. G., Cairncross, B., Rubidge, B. S., Smith, R. M. H., & Hancox, P. J. (2005). The Karoo basins of south-central Africa. *Journal of African Earth Sciences*, *43*(1–3), 211–253. <https://doi.org/10.1016/j.jafrearsci.2005.07.007>
- Chadwick, O. A., Roering, J. J., Heimsath, A. M., Levick, S. R., Asner, G. P., & Khomo, L. (2013). Shaping post-orogenic landscapes by climate and chemical weathering. *Geology*, *41*(11), 1171–1174. <https://doi.org/10.1130/g34721.1>
- Cockburn, H. A. P., Brown, R. W., Summerfield, M. A., & Seidl, M. A. (2000). Quantifying passive margin denudation and landscape development using a combined fission-track thermochronology and cosmogenic isotope analysis approach. *Earth and Planetary Science Letters*, *179*(3), 429–435. [https://doi.org/10.1016/S0012-821X\(00\)00144-8](https://doi.org/10.1016/S0012-821X(00)00144-8)
- Cockburn, H. A. P., Seidl, M. A., & Summerfield, M. A. (1999). Quantifying denudation rates on inselbergs in the central Namib Desert using in situ-produced cosmogenic ¹⁰Be and ²⁶Al. *Geology*, *27*(5), 399–402. [https://doi.org/10.1130/0091-7613\(1999\)027<0399:qdroi>2.3.co;2](https://doi.org/10.1130/0091-7613(1999)027<0399:qdroi>2.3.co;2)
- Cohen, A. S., Coe, A. L., Harding, S. M., & Schwark, L. (2004). Osmium isotope evidence for the regulation of atmospheric CO₂ by continental weathering. *Geology*, *32*(2), 157–160. <https://doi.org/10.1130/g20158.1>
- Colli, L., Stotz, I., Bunge, H.-P., Smethurst, M., Clark, S., Iaffaldano, G., et al. (2014). Rapid South Atlantic spreading changes and coeval vertical motion in surrounding continents: Evidence for temporal changes of pressure-driven upper mantle flow. *Tectonics*, *33*(7), 1304–1321. <https://doi.org/10.1002/2014tc003612>
- Conrad, C. P., & Molnar, P. (1997). The growth of Rayleigh–Taylor-type instabilities in the lithosphere for various rheological and density structures. *Geophysical Journal International*, *129*(1), 95–112. <https://doi.org/10.1111/j.1365-246x.1997.tb00939.x>
- Cordonnier, G., Bovy, B., & Braun, J. (2019). A versatile, linear complexity algorithm for flow routing in topographies with depressions. *Earth Surface Dynamics*, *7*(2), 549–562. <https://doi.org/10.5194/esurf-7-549-2019>
- Cox, K. G. (1989). The role of mantle plumes in the development of continental drainage patterns. *Nature*, *342*(6252), 873–877. <https://doi.org/10.1038/342873a0>
- Croissant, T., & Braun, J. (2014). Constraining the stream power law: A novel approach combining a landscape evolution model and an inversion method. *Earth Surface Dynamics*, *2*(1), 155–166. <https://doi.org/10.5194/esurf-2-155-2014>
- Crowley, K. d., Cameron, M., & Schaefer, R. I. (1991). Experimental studies of annealing of etched fission tracks in fluorapatite. *Geochimica et Cosmochimica Acta*, *55*(5), 1449–1465. [https://doi.org/10.1016/0016-7037\(91\)90320-5](https://doi.org/10.1016/0016-7037(91)90320-5)
- Dauteuil, O., Bessin, P., & Guillocheau, F. (2015). Topographic growth around the Orange River valley, southern Africa: A Cenozoic record of crustal deformation and climatic change. *Geomorphology*, *233*, 5–19. <https://doi.org/10.1016/j.geomorph.2014.11.017>
- Decker, J. E., Niedermann, S., & de Wit, M. J. (2013). Climatically influenced denudation rates of the southern African plateau: Clues to solving a geomorphic paradox. *Geomorphology*, *190*, 48–60. <https://doi.org/10.1016/j.geomorph.2013.02.007>
- De Putter, T., & Ruffet, G. (2020). Supergene manganese ore records 75 Myr-long Campanian to Pleistocene geodynamic evolution and weathering history of the Central African Great Lakes Region—Tectonics drives, climate assists. *Gondwana Research*. <https://doi.org/10.1016/j.gr.2020.01.021>
- Dessert, C., Dupré, B., Gaillardet, J., François, L. M., & Allègre, C. J. (2003). Basalt weathering laws and the impact of basalt weathering on the global carbon cycle. *Chemical Geology*, *202*(3–4), 257–273. <https://doi.org/10.1016/j.chemgeo.2002.10.001>
- de Wit, M. (2007). The Kalahari Epeirogeny and climate change: Differentiating cause and effect from core to space. *South African Journal of Geology*, *110*(2–3), 367–392. <https://doi.org/10.2113/gssaj.110.2-3.367>

- De Wit, M. C. J. (1988). Aspects of the geomorphology of the north-western Cape, South Africa. In *Geomorphological studies in southern Africa* (pp. 57–69). CRC Press.
- de Wit, M. C. J. (1999). Post-Gondwana drainage and the development of diamond placers in western South Africa. *Economic Geology*, 94(5), 721–740. <https://doi.org/10.2113/gsecongeo.94.5.721>
- Ding, X., Salles, T., Flament, N., Mallard, C., & Rey, P. F. (2019). Drainage and sedimentary responses to dynamic topography. *Geophysical Research Letters*, 46(24), 14385–14394. <https://doi.org/10.1029/2019gl084400>
- Dingle, R., & Hendry, Q. (1984). Late Mesozoic and Tertiary sediment supply to the Eastern Cape Basin (SE Atlantic) and palaeo-drainage systems in southwestern Africa. *Marine Geology*, 56(1–4), 13–26. [https://doi.org/10.1016/0025-3227\(84\)90003-3](https://doi.org/10.1016/0025-3227(84)90003-3)
- Dingle, R. V., & Scrutton, R. A. (1974). Continental breakup and the development of post-paleozoic sedimentary basins around Southern Africa. *GSA Bulletin*, 85(9), 1467–1474. [https://doi.org/10.1130/0016-7606\(1974\)85<1467:cbatdo>2.0.co;2](https://doi.org/10.1130/0016-7606(1974)85<1467:cbatdo>2.0.co;2)
- Dirks, P. H. G. M., Placzek, C. J., Fink, D., Dosseto, A., & Roberts, E. (2016). Using ¹⁰Be cosmogenic isotopes to estimate erosion rates and landscape changes during the Plio-Pleistocene in the Cradle of Humankind, South Africa. *Journal of Human Evolution*, 96, 19–34. <https://doi.org/10.1016/j.jhevol.2016.03.002>
- Dixey, F. (1955). *Some aspects of the geomorphology of central and southern Africa*. Geological Society of South Africa.
- Doucouré, C. M., & de Wit, M. J. (2003). Old inherited origin for the present near-bimodal topography of Africa. *Journal of African Earth Sciences*, 36(4), 371–388. [https://doi.org/10.1016/s0899-5362\(03\)00019-8](https://doi.org/10.1016/s0899-5362(03)00019-8)
- Doucouré, C. M., de Wit, M. J., & Mushayandebvu, M. F. (1996). Effective elastic thickness of the continental lithosphere in South Africa. *Journal of Geophysical Research*, 101(B5), 11291–11303. <https://doi.org/10.1029/95jb03718>
- Duncan, R. A., Hooper, P. R., Rehacek, J., Marsh, J. S., & Duncan, A. R. (1997). The timing and duration of the Karoo igneous event, southern Gondwana. *Journal of Geophysical Research*, 102(B8), 18127–18138. <https://doi.org/10.1029/97jb00972>
- Dupré, B., Dessert, C., Oliva, P., Goddérès, Y., Viers, J., François, L., et al. (2003). Rivers, chemical weathering and Earth's climate. *Comptes Rendus Geoscience*, 335(16), 1141–1160. <https://doi.org/10.1016/j.crte.2003.09.015>
- Ebinger, C. J., & Sleep, N. H. (1998). Cenozoic magmatism throughout east Africa resulting from impact of a single plume. *Nature*, 395(6704), 788–791. <https://doi.org/10.1038/27417>
- Erlanger, E. D., Granger, D. E., & Gibbon, R. J. (2012). Rock uplift rates in South Africa from isochron burial dating of fluvial and marine terraces. *Geology*, 40(11), 1019–1022. <https://doi.org/10.1130/g33172.1>
- Farley, K. (2000). Helium diffusion from apatite: General behavior as illustrated by Durango fluorapatite. *Journal of Geophysical Research*, 105(B2), 2903–2914. <https://doi.org/10.1029/1999jb900348>
- Flament, N., Gurnis, M., & Müller, R. D. (2013). A review of observations and models of dynamic topography. *Lithosphere*, 5(2), 189–210. <https://doi.org/10.1130/l245.1>
- Flament, N., Gurnis, M., Williams, S., Seton, M., Skogseid, J., Heine, C., & Dietmar Müller, R. (2014). Topographic asymmetry of the South Atlantic from global models of mantle flow and lithospheric stretching. *Earth and Planetary Science Letters*, 387, 107–119. <https://doi.org/10.1016/j.epsl.2013.11.017>
- Fleming, A., Summerfield, M. A., Stone, J. O., Fifield, L. K., & Cresswell, R. G. (1999). Denudation rates for the southern Drakensberg escarpment, SE Africa, derived from in-situ-produced cosmogenic ³⁶Cl: Initial results. *Journal of the Geological Society*, 156(2), 209–212. <https://doi.org/10.1144/gsjgs.156.2.0209>
- Flowers, R. M., Ketcham, R. A., Shuster, D. L., & Farley, K. A. (2009). Apatite (U–Th)/He thermochronometry using a radiation damage accumulation and annealing model. *Geochimica et Cosmochimica Acta*, 73(8), 2347–2365. <https://doi.org/10.1016/j.gca.2009.01.015>
- Flowers, R. M., & Schoene, B. (2010). (U–Th)/He thermochronometry constraints on unroofing of the eastern Kaapvaal craton and significance for uplift of the southern African Plateau. *Geology*, 38(9), 827–830. <https://doi.org/10.1130/g30980.1>
- Gallagher, K., & Brown, R. W. (1999a). Denudation and uplift at passive margins: The record on the Atlantic Margin of southern Africa. *Philosophical Transactions of the Royal Society of London, Series A: Mathematical, Physical and Engineering Sciences*, 357(1753), 835–859. <https://doi.org/10.1098/rsta.1999.0354>
- Gallagher, K., & Brown, R. W. (1999b). The Mesozoic denudation history of the Atlantic margins of southern Africa and southeast Brazil and the relationship to offshore sedimentation. *Geological Society, London, Special Publications*, 153(1), 41–53. <https://doi.org/10.1144/GSL.SP.1999.153.01.03>
- Garzanti, E., Dinis, P., Vermeesch, P., Andò, S., Hahn, A., Huvi, J., et al. (2018). Sedimentary processes controlling ultralong cells of littoral transport: Placer formation and termination of the Orange sand highway in southern Angola. *Sedimentology*, 65(2), 431–460. <https://doi.org/10.1111/sed.12387>
- Garzanti, E., Resentini, A., Andò, S., Vezzoli, G., Pereira, A., & Vermeesch, P. (2015). Physical controls on sand composition and relative durability of detrital minerals during ultra-long distance littoral and aeolian transport (Namibia and southern Angola). *Sedimentology*, 62(4), 971–996. <https://doi.org/10.1111/sed.12169>
- Gilchrist, A. R., Kooi, H., & Beaumont, C. (1994). Post-Gondwana geomorphic evolution of southwestern Africa: Implications for the controls on landscape development from observations and numerical experiments. *Journal of Geophysical Research*, 99(B6), 12211–12228. <https://doi.org/10.1029/94jb00046>
- Gilchrist, A. R., & Summerfield, M. A. (1990). Differential denudation and flexural isostasy in formation of rifted-margin upwarps. *Nature*, 346(6286), 739–742. <https://doi.org/10.1038/346739a0>
- Glotzbach, C., Paape, A., Baade, J., Reinwarth, B., Rowntree, K., & Miller, J. (2016). Cenozoic landscape evolution of the Kruger National Park as derived from cosmogenic nuclide analyses. *Terra Nova*, 28(5), 316–322. <https://doi.org/10.1111/ter.12223>
- Göğüş, O. H., & Pysklywec, R. N. (2008a). Mantle lithosphere delamination driving plateau uplift and synconvergent extension in eastern Anatolia. *Geology*, 36(9), 723–726. <https://doi.org/10.1130/G24982A.1>
- Göğüş, O. H., & Pysklywec, R. N. (2008b). Near-surface diagnostics of dripping or delaminating lithosphere. *Journal of Geophysical Research*, 113(B11). <https://doi.org/10.1029/2007JB005123>
- Green, P. F., Duddy, I., Gleadow, A., Tingate, P., & Laslett, G. (1986). Thermal annealing of fission tracks in apatite: 1. A qualitative description. *Chemical Geology: Isotope Geoscience Section*, 59, 237–253. [https://doi.org/10.1016/0168-9622\(86\)90074-6](https://doi.org/10.1016/0168-9622(86)90074-6)
- Green, P. F., Duddy, I. R., Japsen, P., Bonow, J. M., & Malan, J. A. (2017). Post-breakup burial and exhumation of the southern margin of Africa. *Basin Research*, 29(1), 96–127. <https://doi.org/10.1111/bre.12167>
- Guillocheau, F., Rouby, D., Robin, C., Helm, C., Rolland, N., Le Carlier de Veslud, C., & Braun, J. (2012). Quantification and causes of the terrigenous sediment budget at the scale of a continental margin: A new method applied to the Namibia-South Africa margin: Quantification and causes of the terrigenous sediment budget at the scale of a continental margin. *Basin Research*, 24(1), 3–30. <https://doi.org/10.1111/j.1365-2117.2011.00511.x>

- Guillocheau, F., Simon, B., Baby, G., Bessin, P., Robin, C., & Dauteuil, O. (2018). Planation surfaces as a record of mantle dynamics: The case example of Africa. *Gondwana Research*, 53, 82–98. <https://doi.org/10.1016/j.gr.2017.05.015>
- Gurnis, M., Mitrovica, J. X., Ritsema, J., & Heijst, H.-J. V. (2000). Constraining mantle density structure using geological evidence of surface uplift rates: The case of the African Superplume. *Geochemistry, Geophysics, Geosystems*, 1(7). <https://doi.org/10.1029/1999gc000035>
- Haddon, I. G., & McCarthy, T. S. (2005). The Mesozoic-Cenozoic interior sag basins of Central Africa: The Late-Cretaceous-Cenozoic Kalahari and Okavango basins. *Journal of African Earth Sciences*, 43(1–3), 316–333. <https://doi.org/10.1016/j.jafrearsci.2005.07.008>
- Hansma, J., Tohver, E., Schrank, C., Jourdan, F., & Adams, D. (2016). The timing of the Cape Orogeny: New ⁴⁰Ar/³⁹Ar age constraints on deformation and cooling of the Cape Fold Belt, South Africa. *Gondwana Research*, 32, 122–137. <https://doi.org/10.1016/j.gr.2015.02.005>
- Hanson, E. K., Moore, J. M., Bordy, E. M., Marsh, J. S., Howarth, G., & Robey, J. V. A. (2009). Cretaceous erosion in Central South Africa: Evidence from upper-crustal xenoliths in Kimberlite Diatremes. *South African Journal of Geology*, 112(2), 125–140. <https://doi.org/10.2113/gssajg.112.2.125>
- Hawthorne, J. (1975). Model of a kimberlite pipe. In *Physics and chemistry of the Earth* (pp. 1–15). Elsevier. <https://doi.org/10.1016/b978-0-08-018017-5.50005-5>
- Hoggard, M. J., White, N., & Al-Attar, D. (2016). Global dynamic topography observations reveal limited influence of large-scale mantle flow. *Nature Geoscience*, 9(6), 456–463. <https://doi.org/10.1038/ngeo2709>
- Holtar, E., & Forsberg, A. W. (2000). *AAPG memoir 73, chapter 29: Postrift development of the Walvis Basin, Namibia: Results from the exploration campaign in quadrant 1911*.
- Hopkins, A. E. (2006). *Seismic stratigraphic interpretation of contourite systems*.
- Howard, A. D., & Kerby, G. (1983). Channel changes in badlands. *The Geological Society of America Bulletin*, 94(6), 739–752. [https://doi.org/10.1130/0016-7606\(1983\)94<739:ccib>2.0.co;2](https://doi.org/10.1130/0016-7606(1983)94<739:ccib>2.0.co;2)
- Howard, A. D., & Tierney, H. E. (2012). Taking the measure of a landscape: Comparing a simulated and natural landscape in the Virginia Coastal Plain. *Geomorphology*, 137(1), 27–40. <https://doi.org/10.1016/j.geomorph.2010.09.031>
- Hu, J., Liu, L., Faccenda, M., Zhou, Q., Fischer, K. M., Marshak, S., & Lundstrom, C. (2018). Modification of the Western Gondwana craton by plume–lithosphere interaction. *Nature Geoscience*, 11(3), 203–210. <https://doi.org/10.1038/s41561-018-0064-1>
- Ibbitt, R. P., Willgoose, G. R., & Duncan, M. J. (1999). Channel network simulation models compared with data from the Ashley River, New Zealand. *Water Resources Research*, 35(12), 3875–3890. <https://doi.org/10.1029/1999wr900245>
- Jelsma, H. A., De Wit, M. J., Thiar, C., Dirks, P. H. G. M., Viola, G., Basson, I. J., & Anckar, E. (2004). Preferential distribution along transcontinental corridors of kimberlites and related rocks of Southern Africa. *South African Journal of Geology*, 107(1–2), 301–324. <https://doi.org/10.2113/107.1-2.301>
- Jenkyns, H. C., Forster, A., Schouten, S., & Sinninghe Damsté, J. S. (2004). High temperatures in the Late Cretaceous Arctic Ocean. *Nature*, 432(7019), 888–892. <https://doi.org/10.1038/nature03143>
- Johnson, M. R., Van Vuuren, C. J., Hegenberger, W. F., Key, R., & Show, U. (1996). Stratigraphy of the Karoo Supergroup in southern Africa: An overview. *Journal of African Earth Sciences*, 23(1), 3–15. [https://doi.org/10.1016/s0899-5362\(96\)00048-6](https://doi.org/10.1016/s0899-5362(96)00048-6)
- Jones, M. Q. W. (1987). Heat flow and heat production in the Namaqua Mobile Belt, South Africa. *Journal of Geophysical Research*, 92(B7), 6273–6289. <https://doi.org/10.1029/jb092ib07p06273>
- Jones, M. Q. W. (2017). Heat flow in the Bushveld Complex, South Africa: Implications for upper mantle structure. *South African Journal of Geology*, 120(3), 351–370. <https://doi.org/10.25131/gssajg.120.3.351>
- Jourdan, F., Féraud, G., Bertrand, H., Watkeys, M., & Renne, P. (2008). The ⁴⁰Ar/³⁹Ar ages of the sill complex of the Karoo large igneous province: Implications for the Pliensbachian-Toarcian climate change. *Geochemistry, Geophysics, Geosystems*, 9(6). <https://doi.org/10.1029/2008gc001994>
- Keen-Zebert, A., Tooth, S., & Stuart, F. M. (2016). Cosmogenic ³He measurements provide insight into lithologic controls on bedrock channel incision: Examples from the South African interior. *The Journal of Geology*, 124(3), 423–434. <https://doi.org/10.1086/685506>
- King, L. C. (1942). *South African scenery. A textbook of geomorphology*.
- King, L. C. (1950). The study of the world's plainlands: A new approach in geomorphology. *Quarterly Journal of the Geological Society*, 106(1–4), 101–131. <https://doi.org/10.1144/gsl.jgs.1950.106.01-04.06>
- Kirby, E., & Whipple, K. X. (2012). Expression of active tectonics in erosional landscapes. *Journal of Structural Geology*, 44, 54–75. <https://doi.org/10.1016/j.jsg.2012.07.009>
- Kounov, A., Niedermann, S., De Wit, M. J., Codilean, A. T., Viola, G., Andreoli, M., & Christl, M. (2015). Cosmogenic ²¹Ne and ¹⁰Be reveal a more than 2 Ma alluvial fan flanking the CAPE Mountains, South Africa. *South African Journal of Geology*, 118(2), 129–144. <https://doi.org/10.2113/gssajg.118.2.129>
- Kounov, A., Niedermann, S., de Wit, M. J., Viola, G., Andreoli, M., & Erzinger, J. (2007). Present denudation rates at selected sections of the South African escarpment and the elevated continental interior based on cosmogenic ³He and ²¹Ne. *South African Journal of Geology*, 110(2–3), 235–248. <https://doi.org/10.2113/gssajg.110.2-3.235>
- Kounov, A., Viola, G., de Wit, M., & Andreoli, M. A. G. (2009). Denudation along the Atlantic passive margin: New insights from apatite fission-track analysis on the western coast of South Africa. *Geological Society, London, Special Publications*, 324(1), 287–306. <https://doi.org/10.1144/sp324.19>
- Kounov, A., Viola, G., Dunkl, I., & Frimmel, H. E. (2013). Southern African perspectives on the long-term morpho-tectonic evolution of cratonic interiors. *Tectonophysics*, 601, 177–191. <https://doi.org/10.1016/j.tecto.2013.05.009>
- Linol, B., & De Wit, M. J. (2016). *Origin and evolution of the Cape Mountains and Karoo Basin*. Springer.
- Lithgow-Bertelloni, C., & Silver, P. G. (1998). Dynamic topography, plate driving forces and the African superswell. *Nature*, 395(6699), 269–272. <https://doi.org/10.1038/26212>
- Macdonald, D., Gomez-Perez, I., Franzese, J., Spalletti, L., Lawver, L., Gahagan, L., et al. (2003). Mesozoic break-up of SW Gondwana: Implications for regional hydrocarbon potential of the southern South Atlantic. *Marine and Petroleum Geology*, 20(3–4), 287–308. [https://doi.org/10.1016/s0264-8172\(03\)00045-x](https://doi.org/10.1016/s0264-8172(03)00045-x)
- Macgregor, D. S. (2020). Regional variations in geothermal gradient and heat flow across the African plate. *Journal of African Earth Sciences*, 171, 103950. <https://doi.org/10.1016/j.jafrearsci.2020.103950>
- Makhubela, T. V., Kramers, J. D., Scherler, D., Wittmann, H., Dirks, P. H. G. M., & Winkler, S. R. (2019). Effects of long soil surface residence times on apparent cosmogenic nuclide denudation rates and burial ages in the Cradle of Humankind, South Africa. *Earth Surface Processes and Landforms*, 44(15), 2968–2981. <https://doi.org/10.1002/esp.4723>
- Margirier, A., Braun, J., Gautheron, C., Carcaillet, J., Schwartz, S., Pinna Jamme, R., & Stanley, J. (2019). Climate control on Early Cenozoic denudation of the Namibian margin as deduced from new thermochronological constraints. *Earth and Planetary Science Letters*, 527, 115779. <https://doi.org/10.1016/j.epsl.2019.115779>

- Marsh, J., Hooper, P., Rehacek, J., Duncan, R., & Duncan, A. (1997). Stratigraphy and age of Karoo basalts of Lesotho and implications for correlations within the Karoo igneous province. *Geophysical Monograph-American Geophysical Union*, 100, 247–272.
- Martin, A. K., Goodlad, S. W., Hartnady, C. J. H., & Plessis, A. du. (1982). Cretaceous palaeopositions of the Falkland Plateau relative to southern Africa using Mesozoic seafloor spreading anomalies. *Geophysical Journal International*, 71(3), 567–579. <https://doi.org/10.1111/j.1365-246x.1982.tb02784.x>
- McMillan, I. (1990). A foraminiferal biostratigraphy and chronostratigraphy for the Pliocene to Pleistocene Upper Algoa Group, Eastern Cape, South Africa. *South African Journal of Geology*, 93(4), 622.
- Molnar, P., Houseman, G. A., & Conrad, C. P. (1998). Rayleigh–Taylor instability and convective thinning of mechanically thickened lithosphere: Effects of non-linear viscosity decreasing exponentially with depth and of horizontal shortening of the layer. *Geophysical Journal International*, 133(3), 568–584. <https://doi.org/10.1046/j.1365-246x.1998.00510.x>
- Moore, A., & Verwoerd, W. (1985). The olivine melilitite–“kimberlite”–carbonatite suite of Namaqualand and Bushmanland, South Africa. *Transactions of the Geological Society of South Africa*, 88(2), 281–294.
- Moore, A. E. (1999). A reappraisal of epeirogenic flexure axes in southern Africa. *South African Journal of Geology*, 102(4), 14.
- Moore, A. E., Blenkinsop, T., & Cotterill, F. W. (2009). Southern African topography and erosion history: Plumes or plate tectonics? *Terra Nova*, 21(4), 310–315. <https://doi.org/10.1111/j.1365-3121.2009.00887.x>
- Morgan-Wall, T. (2020). *Rayshader: Create maps and visualize data in 2D and 3D*. Retrieved from <https://CRAN.R-project.org/package=rayshader>
- Moucha, R., & Forte, A. M. (2011). Changes in African topography driven by mantle convection. *Nature Geoscience*, 4(10), 707–712. <https://doi.org/10.1038/ngeo1235>
- Müller, R. D., Royer, J.-Y., & Lawver, L. A. (1993). Revised plate motions relative to the hotspots from combined Atlantic and Indian Ocean hotspot tracks. *Geology*, 21(3), 275–278. [https://doi.org/10.1130/0091-7613\(1993\)021<0275:rpmrtt>2.3.co;2](https://doi.org/10.1130/0091-7613(1993)021<0275:rpmrtt>2.3.co;2)
- Nakashole, A. N., Hodgson, D. M., Chapman, R. J., Morgan, D. J., & Jacob, R. J. (2018). Long-term controls on continental-scale Bedrock River terrace deposition from integrated clast and heavy mineral assemblage analysis: An example from the lower Orange River, Namibia. *Sedimentary Geology*, 364, 103–120. <https://doi.org/10.1016/j.sedgeo.2017.12.010>
- Nunn, J. A., & Aires, J. R. (1988). Gravity anomalies and flexure of the lithosphere at the Middle Amazon Basin, Brazil. *Journal of Geophysical Research*, 93(B1), 415–428. <https://doi.org/10.1029/jb093ib01p00415>
- Nyblade, A. A., & Sleep, N. H. (2003). Long lasting epeirogenic uplift from mantle plumes and the origin of the Southern African Plateau. *Geochemistry, Geophysics, Geosystems*, 4(12). <https://doi.org/10.1029/2003gc000573>
- O’Neill, C., Müller, D., & Steinberger, B. (2005). On the uncertainties in hot spot reconstructions and the significance of moving hot spot reference frames. *Geochemistry, Geophysics, Geosystems*, 6(4). <https://doi.org/10.1029/2004GC000784>
- Osei Tutu, A., Steinberger, B., Sobolev, S. V., Rogozhina, I., & Popov, A. A. (2018). Effects of upper mantle heterogeneities on the lithospheric stress field and dynamic topography. *Solid Earth*, 9(3), 649–668. <https://doi.org/10.5194/se-9-649-2018>
- Partridge, T. C., Dollar, E. S. J., Moolman, J., & Dollar, L. H. (2010). The geomorphic provinces of South Africa, Lesotho and Swaziland: A physiographic subdivision for earth and environmental scientists. *Transactions of the Royal Society of South Africa*, 65(1), 1–47. <https://doi.org/10.1080/00359191003652033>
- Partridge, T. C., & Maud, R. R. (1987). Geomorphic evolution of southern Africa since the Mesozoic. *South African Journal of Geology*, 90(2), 179–208.
- Paton, D. A., van der Spuy, D., di Primio, R., & Horsfield, B. (2008). Tectonically induced adjustment of passive-margin accommodation space; influence on the hydrocarbon potential of the Orange Basin, South Africa. *AAPG Bulletin*, 92(5), 589–609. <https://doi.org/10.1306/12280707023>
- Paul, J. D., Roberts, G. G., & White, N. (2014). The African landscape through space and time. *Tectonics*, 33(6), 898–935. <https://doi.org/10.1002/2013tc003479>
- Pérez-Gussinyé, M., Metois, M., Fernández, M., Vergés, J., Fullea, J., & Lowry, A. R. (2009). Effective elastic thickness of Africa and its relationship to other proxies for lithospheric structure and surface tectonics. *Earth and Planetary Science Letters*, 287(1), 152–167. <https://doi.org/10.1016/j.epsl.2009.08.004>
- Phillips, D., & Harris, J. W. (2009). Diamond provenance studies from 40Ar/39Ar dating of clinopyroxene inclusions: An example from the west coast of Namibia. *Lithos*, 112, 793–805. <https://doi.org/10.1016/j.lithos.2009.05.003>
- Phillips, D., Harris, J. W., de Wit, M. C. J., & Matchan, E. L. (2018). Provenance history of detrital diamond deposits, West Coast of Namaqualand, South Africa. *Mineralogy and Petrology*, 112(S1), 259–273. <https://doi.org/10.1007/s00710-018-0568-9>
- Pickford, M., Eisenmann, V., & Senut, B. (1999). *Timing of landscape development and calcrete genesis in Northern Namaqualand* (Vol. 3).
- Ponte, J.-P., Robin, C., Guillocheau, F., Popescu, S., Suc, J.-P., Dall’Asta, M., et al. (2019). The Zambezi delta (Mozambique channel, East Africa): High resolution dating combining bio-orbital and seismic stratigraphies to determine climate (palaeoprecipitation) and tectonic controls on a passive margin. *Marine and Petroleum Geology*, 105, 293–312. <https://doi.org/10.1016/j.marpetgeo.2018.07.017>
- Pysklywec, R. N., & Mitrovica, J. X. (1999). The role of subduction-induced subsidence in the evolution of the Karoo Basin. *The Journal of Geology*, 107(2), 155–164. <https://doi.org/10.1086/314338>
- Raab, M. J. (2001). *The geomorphic response of the passive continental margin of northern Namibia to Gondwana break-up and global scale tectonics* (PhD). Georg-August-Universität zu Göttingen.
- Raab, M. J., Brown, R. W., Gallagher, K., Carter, A., & Weber, K. (2002). Late Cretaceous reactivation of major crustal shear zones in northern Namibia: Constraints from apatite fission track analysis. *Tectonophysics*, 349(1–4), 75–92. [https://doi.org/10.1016/S0040-1951\(02\)00047-1](https://doi.org/10.1016/S0040-1951(02)00047-1)
- Raab, M. J., Brown, R. W., Gallagher, K., Weber, K., & Gleadow, A. J. W. (2005). Denudational and thermal history of the Early Cretaceous Brandberg and Okenyanya igneous complexes on Namibia’s Atlantic passive margin: Exhumation of Namibia’s passive margin. *Tectonics*, 24(3). <https://doi.org/10.1029/2004tc001688>
- Renne, P. R., Glen, J. M., Milner, S. C., & Duncan, A. R. (1996). Age of Etendeka flood volcanism and associated intrusions in southwestern Africa. *Geology*, 24(7), 659–662. [https://doi.org/10.1130/0091-7613\(1996\)024<0659:aeofva>2.3.co;2](https://doi.org/10.1130/0091-7613(1996)024<0659:aeofva>2.3.co;2)
- Richardson, J. C., Hodgson, D. M., Paton, D., Craven, B., Rawcliffe, A., & Lang, A. (2017). Where is my sink? Reconstruction of landscape development in southwestern Africa since the Late Jurassic. *Gondwana Research*, 45, 43–64. <https://doi.org/10.1016/j.gr.2017.01.004>
- Roberts, D. L., Sciscio, L., Herries, A. I., Scott, L., Bamford, M. K., Musekiwa, C., & Tsikos, H. (2013). Miocene fluvial systems and palynofloras at the southwestern tip of Africa: Implications for regional and global fluctuations in climate and ecosystems. *Earth-Science Reviews*, 124, 184–201. <https://doi.org/10.1016/j.earscirev.2013.05.001>
- Roberts, E. M., Stevens, N. J., O’Connor, P. M., Dirks, P. H. G. M., Gottfried, M. D., Clyde, W. C., et al. (2012). Initiation of the western branch of the East African Rift coeval with the eastern branch. *Nature Geoscience*, 5(4), 289–294. <https://doi.org/10.1038/ngeo1432>

- Roberts, G. G., & White, N. (2010). Estimating uplift rate histories from river profiles using African examples. *Journal of Geophysical Research*, 115(B2). <https://doi.org/10.1029/2009jb006692>
- Rouby, D., Bonnet, S., Guillocheau, F., Gallagher, K., Robin, C., Biancotto, F., et al. (2009). Sediment supply to the Orange sedimentary system over the last 150My: An evaluation from sedimentation/denudation balance. *Marine and Petroleum Geology*, 26(6), 782–794. <https://doi.org/10.1016/j.marpetgeo.2008.08.004>
- Rubey, M., Brune, S., Heine, C., Davies, D. R., Williams, S. E., & Müller, R. D. (2017). Global patterns in Earth's dynamic topography since the Jurassic: The role of subducted slabs. *Solid Earth*, 8(5), 899–919. <https://doi.org/10.5194/se-8-899-2017>
- Rudge, J. F., Roberts, G. G., White, N. J., & Richardson, C. N. (2015). Uplift histories of Africa and Australia from linear inverse modeling of drainage inventories: Rudge et al. *Journal of Geophysical Research: Earth Surface*, 120(5), 894–914. <https://doi.org/10.1002/2014jf003297>
- Said, A., Moder, C., Clark, S., & Ghorbal, B. (2015). Cretaceous–Cenozoic sedimentary budgets of the Southern Mozambique Basin: Implications for uplift history of the South African Plateau. *Journal of African Earth Sciences*, 109, 1–10. <https://doi.org/10.1016/j.jafrearsci.2015.05.007>
- Sambidge, M. (1999). Geophysical inversion with a neighbourhood algorithm—I. Searching a parameter space. *Geophysical Journal International*, 138(2), 479–494. <https://doi.org/10.1046/j.1365-246x.1999.00876.x>
- Sandersen, A. (2007). *A palynological investigation of the offshore Cretaceous sequence on the south-west coast of South Africa (PhD)*. University of the Witwatersrand.
- Scharf, T. E., Codilean, A. T., de Wit, M., Jansen, J. D., & Kubik, P. W. (2013). Strong rocks sustain ancient postorogenic topography in southern Africa. *Geology*, 41(3), 331–334. <https://doi.org/10.1130/g33806.1>
- Scheiber-Enslin, S. E., Ebbing, J., & Webb, S. J. (2015). New depth maps of the Main Karoo Basin, used to explore the Cape isostatic anomaly, South Africa. *South African Journal of Geology*, 118(3), 225–248. <https://doi.org/10.2113/gssajg.118.3.225>
- Schmitz, M. D., & Bowring, S. A. (2003). Constraints on the thermal evolution of continental lithosphere from U–Pb accessory mineral thermochronometry of lower crustal xenoliths, southern Africa. *Contributions to Mineralogy and Petrology*, 144(5), 592–618. <https://doi.org/10.1007/s00410-002-0419-9>
- Scholtz, A. (1985). The palynology of the upper lacustrine sediments of the Arnot Pipe, Banke, Namaqualand. *Annals of the South African Museum*, 95(1), 1–109.
- Senut, B., Pickford, M., & Ségalen, L. (2009). Neogene desertification of Africa. *Comptes Rendus Geoscience*, 341(8), 591–602. <https://doi.org/10.1016/j.crte.2009.03.008>
- Shuster, D. L., Flowers, R. M., & Farley, K. A. (2006). The influence of natural radiation damage on helium diffusion kinetics in apatite. *Earth and Planetary Science Letters*, 249(3), 148–161. <https://doi.org/10.1016/j.epsl.2006.07.028>
- Skinner, C. J., Coulthard, T. J., Schwanghart, W., Wiel, M. J. V. D., & Hancock, G. (2018). Global sensitivity analysis of parameter uncertainty in landscape evolution models. *Geoscientific Model Development*, 11(12), 4873–4888. <https://doi.org/10.5194/gmd-11-4873-2018>
- Smith, R. (1986). Sedimentation and palaeoenvironments of Late Cretaceous crater-lake deposits in Bushmanland, South Africa. *Sedimentology*, 33(3), 369–386. <https://doi.org/10.1111/j.1365-3091.1986.tb00542.x>
- Stanley, J. R. (2020). Model inputs and results from FastScape landscape evolution model runs for southern Africa [Data set]. *Zenodo*. <https://doi.org/10.5281/zenodo.4153802>
- Stanley, J. R., & Flowers, R. M. (2020). Mesozoic denudation history of the lower Orange River and eastward migration of erosion across the southern African Plateau. *Lithosphere*. <https://doi.org/10.1130/L1121.1>
- Stanley, J. R., Flowers, R. M., & Bell, D. R. (2013). Kimberlite (U–Th)/He dating links surface erosion with lithospheric heating, thinning, and metasomatism in the southern African Plateau. *Geology*, 41(12), 1243–1246. <https://doi.org/10.1130/g34797.1>
- Stanley, J. R., Flowers, R. M., & Bell, D. R. (2015). Erosion patterns and mantle sources of topographic change across the southern African Plateau derived from the shallow and deep records of kimberlites. *Geochemistry, Geophysics, Geosystems*, 16(9), 3235–3256. <https://doi.org/10.1002/2015gc005969>
- Steinberger, B. (2016). Topography caused by mantle density variations: Observation-based estimates and models derived from tomography and lithosphere thickness. *Geophysical Journal International*, 205(1), 604–621. <https://doi.org/10.1093/gji/ggw040>
- Steinberger, B., Conrad, C. P., Osei Tutu, A., & Hoggard, M. J. (2019). On the amplitude of dynamic topography at spherical harmonic degree two. *Tectonophysics*, 760, 221–228. <https://doi.org/10.1016/j.tecto.2017.11.032>
- Steinberger, B., & Torsvik, T. H. (2008). Absolute plate motions and true polar wander in the absence of hotspot tracks. *Nature*, 452(7187), 620–623. <https://doi.org/10.1038/nature06824>
- Stevenson, I. R., & McMillan, I. K. (2004). Incised valley fill stratigraphy of the Upper Cretaceous succession, proximal Orange Basin, Atlantic margin of southern Africa. *Journal of the Geological Society*, 161(2), 185–208. <https://doi.org/10.1144/0016-764902-003>
- Summerfield, M. A. (1983). Silcrete as a paleoclimatic indicator: Evidence from southern Africa. *Palaeogeography, Palaeoclimatology, Palaeoecology*, 41(1), 65–79. [https://doi.org/10.1016/0031-0182\(83\)90076-7](https://doi.org/10.1016/0031-0182(83)90076-7)
- Svensen, H., Corfu, F., Polteau, S., Hammer, Ø., & Planke, S. (2012). Rapid magma emplacement in the Karoo Large Igneous Province. *Earth and Planetary Science Letters*, 325–326, 1–9. <https://doi.org/10.1016/j.epsl.2012.01.015>
- ten Brink, U., & Stern, T. (1992). Rift flank uplifts and Hinterland Basins: Comparison of the Transantarctic Mountains with the Great Escarpment of southern Africa. *Journal of Geophysical Research*, 97(B1), 569–585. <https://doi.org/10.1029/91jb02231>
- Tennekes, M. (2018). tmap: Thematic maps in R. *Journal of Statistical Software*, 84(6), 1–39. <https://doi.org/10.18637/jss.v084.i06>
- Thiéblemont, A., Hernandez-Molina, F. J., Ponte, J.-P., Robin, C., Guillocheau, F., Cazola, C., & Raison, F. (2020). Seismic stratigraphic framework and depositional history for Cretaceous and Cenozoic contourite depositional systems of the Mozambique Channel, SW Indian Ocean. *Marine Geology*, 425, 106192. <https://doi.org/10.1016/j.margeo.2020.106192>
- Tinker, J., de Wit, M., & Brown, R. W. (2008a). Linking source and sink: Evaluating the balance between onshore erosion and offshore sediment accumulation since Gondwana break-up, South Africa. *Tectonophysics*, 455(1–4), 94–103. <https://doi.org/10.1016/j.tecto.2007.11.040>
- Tinker, J., de Wit, M., & Brown, R. W. (2008b). Mesozoic exhumation of the southern Cape, South Africa, quantified using apatite fission track thermochronology. *Tectonophysics*, 455(1–4), 77–93. <https://doi.org/10.1016/j.tecto.2007.10.009>
- Uenzelmann-Neben, G., Schlüter, P., & Weigelt, E. (2007). Cenozoic oceanic circulation within the South African gateway: Indications from seismic stratigraphy. *South African Journal of Geology*, 110(2–3), 275–294. <https://doi.org/10.2113/gssajg.110.2-3.275>
- Vafeas, N. A., Bignon, L. C., Viljoen, K. S., & Meffre, S. (2018). New evidence for the early onset of supergene alteration along the Kalahari unconformity. *South African Journal of Geology*, 121(2), 157–170. <https://doi.org/10.25131/sajg.121.0012>
- Van Der Beek, P., Summerfield, M. A., Braun, J., Brown, R. W., & Fleming, A. (2002). Modeling postbreakup landscape development and denudational history across the southeast African (Drakensberg Escarpment) margin. *Journal of Geophysical Research*, 107(B12). <https://doi.org/10.1029/2001jb000744>

- Ward, J. (1988). Eolian, fluvial and pan (playa) facies of the Tertiary Tsondab Sandstone Formation in the central Namib Desert, Namibia. *Sedimentary Geology*, 55(1–2), 143–162. [https://doi.org/10.1016/0037-0738\(88\)90094-2](https://doi.org/10.1016/0037-0738(88)90094-2)
- Watkins, C. E., & Conrad, C. P. (2018). Constraints on dynamic topography from asymmetric subsidence of the mid-ocean ridges. *Earth and Planetary Science Letters*, 484, 264–275. <https://doi.org/10.1016/j.epsl.2017.12.028>
- Whipple, K. X. (2004). Bedrock rivers and the geomorphology of active orogens. *Annual Review of Earth and Planetary Sciences*, 32(1), 151–185. <https://doi.org/10.1146/annurev.earth.32.101802.120356>
- Whipple, K. X., & Tucker, G. E. (1999). Dynamics of the stream-power river incision model: Implications for height limits of mountain ranges, landscape response timescales, and research needs. *Journal of Geophysical Research*, 104(B8), 17661–17674. <https://doi.org/10.1029/1999jb900120>
- Wickham, H. (2016). *ggplot2: Elegant graphics for data analysis*. Springer-Verlag. Retrieved from <https://ggplot2.tidyverse.org>
- Wildman, M., Brown, R., Persano, C., Beucher, R., Stuart, F. M., Mackintosh, V., et al. (2017). Contrasting Mesozoic evolution across the boundary between on and off craton regions of the South African plateau inferred from apatite fission track and (U-Th-Sm)/He thermochronology: Mesozoic Evolution of Southern Africa. *Journal of Geophysical Research: Solid Earth*, 122(2), 1517–1547. <https://doi.org/10.1002/2016jb013478>
- Wildman, M., Brown, R. W., Beucher, R., Persano, C., Stuart, F., Gallagher, K., et al. (2016). The chronology and tectonic style of landscape evolution along the elevated Atlantic continental margin of South Africa resolved by joint apatite fission track and (U-Th-Sm)/He thermochronology: Evolution of SW African Passive Margin. *Tectonics*, 35(3), 511–545. <https://doi.org/10.1002/2015tc004042>
- Wildman, M., Brown, R. W., Watkins, R., Carter, A., Gleadow, A., & Summerfield, M. (2015). Post break-up tectonic inversion across the southwestern cape of South Africa: New insights from apatite and zircon fission track thermochronometry. *Tectonophysics*, 654, 30–55. <https://doi.org/10.1016/j.tecto.2015.04.012>
- Williams, L. S. (2015). Sedimentology of the Lower Cretaceous reservoirs of the Sea Lion Field, North Falkland Basin. *Petroleum Geoscience*, 21(2–3), 183–198. <https://doi.org/10.1144/petgeo2014-039>
- Winterbourne, J., Crosby, A., & White, N. (2009). Depth, age and dynamic topography of oceanic lithosphere beneath heavily sedimented Atlantic margins. *Earth and Planetary Science Letters*, 287(1–2), 137–151. <https://doi.org/10.1016/j.epsl.2009.08.019>
- Zhang, N., Zhong, S., & Flowers, R. M. (2012). Predicting and testing continental vertical motion histories since the Paleozoic. *Earth and Planetary Science Letters*, 317–318, 426–435. <https://doi.org/10.1016/j.epsl.2011.10.041>

References From the Supporting Information

- Chumakov, N. M., Zharkov, M. A., Herman, A. B., Doludenko, M. P., Kalandadze, N. N., Lebedev, E. L., et al. (1995). Climatic Belts of the Mid-Cretaceous Time. *Stratigraphy and Geological Correlation*, 3(3), 42–63.
- Dietrich, P., & Hofmann, A. (2019). Ice-margin fluctuation sequences and grounding zone wedges: The record of the Late Palaeozoic Ice Age in the eastern Karoo Basin (Dwyka Group, South Africa). *The Depositional Record*, 5(2), 247–271. <https://doi.org/10.1002/dep2.74>
- Hay, W. W., & Floegel, S. (2012). New thoughts about the Cretaceous climate and oceans. *Earth-Science Reviews*, 115(4), 262–272. <https://doi.org/10.1016/j.earscirev.2012.09.008>
- Rayner, R. J., Bamford, M. K., Brothers, D. J., Dippenaar-Schoeman, A. S., McKay, I. J., Oberprieler, R. G., & Waters, S. B. (1997). Cretaceous fossils from the Orapa diamond mine. *Palaeontologia Africana*, 33, 55–65.